

Disclaimer: *This is a pre-publication, uncorrected version of the article Zhu et al. accepted for publication in Marine Chemistry. Readers are recommended to consult the final published version for accuracy and citation at <https://doi.org/10.1016/j.marchem.2021.104038>.*

5

Equilibrium calculations of iron speciation and apparent iron solubility in the Celtic Sea at ambient seawater pH using the NICA-Donnan model

10 Kechen Zhu¹, Antony Birchill², Angela Milne², Simon Ussher², Matthew P. Humphreys³, Nealy Carr⁴, Claire Mahaffey⁴, Maeve C. Lohan⁵, Eric P. Achterberg¹ and Martha Gledhill*¹

¹ GEOMAR Helmholtz Center for Ocean Research Kiel, Wischhofstr. 1-3, Kiel, Germany

² School of Geography, Earth and Environmental Sciences, University of Plymouth, Plymouth,
15 UK

³ NIOZ Royal Netherlands Institute for Sea Research, Department of Ocean Systems (OCS),
Texel, The Netherlands

⁴ School of Environmental Sciences, 4 Brownlow Street, University of Liverpool, L69 3GP, UK

⁵ School of Ocean and Earth Science, University of Southampton, Southampton, UK

20

25

* Correspondence: mgledhill@geomar.de

30

1. Abstract

We used a combined ion pairing - organic matter model (NICA-Donnan) to predict the organic complexation of iron (Fe) at ambient pH and temperature in the Celtic Sea. We optimized our model via determination of Fe speciation with Adsorptive Cathodic Stripping Voltammetry using the added Fe-binding ligand 1-nitroso-2-naphthol (HNN) in the presence and absence of natural organic matter. We compared determined Fe speciation with simulated titrations obtained via application of the NICA-Donnan model with four different NICA parameter sets representing a range of binding site strengths and heterogeneities. We tested the assumption that binding sites scale to dissolved organic carbon (DOC) concentrations in marine waters. We found that a constant low DOC concentration resulted in an improved fit of our titration data to the simulated titrations, suggesting that the changes in dissolved organic matter composition that occur alongside changes in DOC concentration dilute the Fe binding site pool. Using the optimal parameter set, we calculated $pFe(III)'$ ($-\log(\sum Fe(OH)_i^{3-i})$) and apparent Fe(III) solubility ($SFe(III)_{app}$) at ambient pH and temperature in the water column of the Celtic Sea. $SFe(III)_{app}$ was defined as the sum of aqueous inorganic Fe(III) species and Fe(III) bound to DOM formed at a free Fe (Fe^{3+}) concentration equal to the limiting solubility of Fe hydroxide ($Fe(OH)_3(s)$). $SFe(III)_{app}$ was within range of the determined dissolved Fe concentrations observed after winter mixing on the shelf and in waters >1500 m depth at our most offshore stations. Our study supports the hypothesis that the ocean dissolved Fe inventory is controlled by the interplay between Fe solubility and Fe binding by organic matter, although the overall number of metal binding sites in the marine environment may not be directly scalable to DOC concentrations.

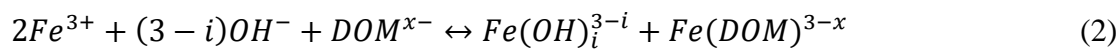
55

60 Keywords: iron complexation, trace metals in the ocean, ocean acidification, intrinsic binding constants, dissolved iron.

2. Introduction

Iron (Fe) is an essential micronutrient for marine phytoplankton growth, and its low supply and solubility limits primary productivity in large parts of the world's ocean (Boyd and Ellwood, 2010). Iron limitation mostly occurs in high –nitrate, low-chlorophyll (HNLC) regions, which make up approximately 30% of the surface ocean (Boyd et al., 2007). However, both Fe limitation and the potential for seasonal Fe limitation have also been reported for coastal regions and shelf seas, including European shelf seas (Birchill et al., 2017; Hogle et al., 2018; Hutchins & Bruland, 1998). The bioavailability and solubility of Fe in seawater is a function of its chemical speciation (Boyd & Ellwood, 2010; Gledhill & Buck, 2012; Hutchins et al., 1999). Inorganic Fe(III) is the thermodynamically favoured form of Fe in oxygenated seawater but, as a result of hydrolysis (equation 1), it has a low solubility that reaches a minimum between pH 7 and 9 (Byrne et al., 2000; Kuma et al., 1996; Liu & Millero, 2002). Hydrolysis competes with binding by organic matter (equation 2), thus complexation by dissolved organic ligands (i.e. those <0.2 µm in size) has the potential to reduce free Fe³⁺ concentrations and consequent formation of insoluble iron hydroxides (Fe(OH)₃(s)) and thereby increase the concentration of Fe(III) observed in the dissolved fraction (<0.2 µm) (Kuma et al., 2000, 1996; Liu and Millero, 2002).

80



Reduction to Fe(II), via e.g. photolysis or biological activity, can also change Fe speciation, potentially increasing both the bioavailability and solubility of Fe (Barbeau et al., 2006; Rose and Waite, 2005; Schlosser et al., 2018). Complexation by organic matter, hydrolysis, and redox speciation thus all play important roles in ocean Fe biogeochemistry, and as a result the global Fe cycle is thought to be influenced by ocean acidification, water column stratification, warming and deoxygenation (Hutchins & Boyd, 2016). Given the role of Fe as an essential micronutrient, there is thus a need to develop reliable approaches that can be used to predict the impact of environmental change on oceanic Fe speciation and biogeochemistry (Ye et al., 2020). Ideally, such approaches would be based on a set of intrinsic thermodynamic and kinetic equations that

90

would describe the chemical speciation and rates of reaction of all Fe species in seawater according to ambient temperature, salinity and pH (Turner et al., 2016; Ye et al., 2020).

95

With respect to Fe(III) speciation in seawater, the work of Liu and Millero (1999) and Byrne et al. (2000) has provided a set of intrinsic thermodynamic constants that describe Fe hydrolysis and the formation of fresh Fe(III)-hydroxide colloidal precipitates (retained on a 0.02 μm filter).

In contrast, for organic complexation, determination of metal speciation in seawater has traditionally adopted an approach where the observed strength and concentrations of metal-binding ligands were related to specific conditions of the sample (i.e. salinity, dissolved Fe concentration) and analysis (i.e. pH typically 8.0-8.2 depending on the method employed). Ocean sections of conditional ligand concentrations published as part of the GEOTRACES research programme (Buck et al., 2018, 2015; Gerringa et al., 2015) showed that, at pH 8 and room temperature, average conditional ligand concentrations range from 1-2 nEq of M Fe, and typically correlate with dissolved Fe concentrations, exceeding them by an average of ca. 1 nEq of M Fe (Caprara et al., 2016). This covariance can at least partially be explained by application of analytical experimental designs and mathematical transformations that simplify a heterogeneous group of binding sites to an “average” site that can be observed under the applied experimental conditions (for further information see e.g. (Gledhill and Gerringa (2017); Van Leeuwen and Town (2005))). Whilst assuming two or more binding sites could overcome the covariance between ligand and dissolved iron concentrations (Buck et al., 2018), results are still specific to the titration pH rather than the sample pH and such assumptions come at the cost of increased parameter uncertainty (Pižeta et al., 2015). Thus, whilst the conditional approach demonstrates that organic complexation is important for the biogeochemistry of Fe, the conditional nature of the obtained results constrains our ability to predict how Fe(III) speciation is likely to change in a future ocean, since it provides no mechanistic knowledge of how Fe(III) binding to organic matter is influenced by pH or temperature.

Exactly how Fe(III) binding to organic matter changes as a function of pH depends on the functional group characteristics of the metal binding components of marine dissolved organic matter (DOM) (Shi et al., 2010; Zhang et al., 2019). Dissolved organic matter is a highly diverse mix of compounds (Koch et al., 2008) that will also potentially change in a future ocean

(Lønborg et al., 2020). Metal binding components likely make up only a minor subset of the overall DOM pool (Zhang et al., 2019). Previous studies have shown that bacteria and phytoplankton can release Fe binding ligands, including siderophores and polysaccharide exudates into their environment (Hassler et al., 2011a; Hassler et al., 2011b; Mawji et al., 2011; Vraspir and Butler, 2009). In addition, ligands can be released following viral lysis (Poorvin et al., 2011) or delivered by terrigenous sources in the form of humic-like substances (Muller, 2018). The organic ligand pool thus shows an intrinsic chemical heterogeneity, which is still not well understood (Gledhill and Buck, 2012), but is likely analogous to metal binding to natural organic matter in terrestrial and freshwater environments (Lodeiro et al., 2020).

Binding models for describing metal binding to organic matter using intrinsic constants (i.e. independent of pH) that account for heterogeneity are widely applied in terrestrial and freshwater environments. Perhaps the most widely used models are the Non-Ideal Competitive Adsorption (NICA)-Donnan model (Kinniburgh et al., 1999), Windermere humic acid model (WHAM) (Tipping et al., 2011), and Stockholm humic model (SHM) (Gustafsson, 2001). A primary assumption in these models is that binding sites scale proportionally to the concentration of dissolved organic carbon (DOC; ‘dissolved’ in this context is typically defined as <0.7 μm in size). The appeal of such an approach lies in the potential for describing the influence of Fe(III) binding to organic matter as a function of ambient pH and DOC concentrations, using a limited set of constants that could be applied to the estimation of Fe speciation across the whole ocean (Hiemstra and van Riemsdijk, 2006; Stockdale et al., 2016). Indeed, a step in this direction has recently been made in Ye et al. (2020), where the NICA-Donnan model has been used to parameterise the impact of future changes in ocean pH on ocean productivity in a global biogeochemical model. The NICA-Donnan model describes the binding behavior of metal ions to a heterogeneous mix of binding sites using a continuous bimodal distribution based on the Langmuir-Freundlich adsorption isotherm (Kinniburgh et al., 1999), while both the WHAM and SHM models rely on a set of empirically derived relationships and a set number of binding sites with different affinities to calculate metal speciation (Gustafsson, 2001; Tipping et al., 2011). A further key difference between the three approaches relates to the application of electrostatic sub-models to describe the impact of ionic strength on binding of metals to the organic matter phase. In the NICA-Donnan model, the Donnan component is used to describe non-specific electrostatic

155 interactions on metal binding to DOM, while the SHM model uses the Basic Stern model
(Gustafsson, 2001) and WHAM uses a correction based on the Debye-Hückel and Gouy-
Chapman theory (Tipping et al., 2011). All three approaches have been successfully used to
predict metal speciation in seawater (Avendaño et al., 2016; Hiemstra & van Riemsdijk, 2006;
Ndungu, 2012; Stockdale et al., 2011, 2015; Tipping et al., 2016). However, since a direct
160 intercomparison study has yet to be undertaken, it is not known if one model is superior to the
others in seawater applications.

In order to further test the applicability of such heterogeneous models to Fe(III) speciation in the
marine environment, we wished to examine predicted and observed relationships between DOC
165 concentrations and Fe speciation in more detail. In this study, we tested the underlying
assumption that Fe speciation determined with a given set of intrinsic NICA constants could be
scaled to different DOC concentrations, at least within the range of DOC concentrations typically
observed in marine waters. In coastal waters, average DOC concentrations are ca. 300 $\mu\text{mol L}^{-1}$
because of enhanced productivity or localized DOC inputs from terrestrial sources (Barrón and
170 Duarte, 2015), while in the open ocean DOC concentrations are lower and vary by at most a
factor of two (40-80 $\mu\text{mol L}^{-1}$, Hansell, 2013). Since DOC composition changes with
concentration (Hansell, 2013), we also implicitly tested a second assumption, that the changes in
DOC composition resulting from microbial utilization of organic matter and giving rise to the
decrease in DOC concentrations in marine environments does not significantly impact the
175 binding properties of Fe. We used samples collected on three cruises in the Celtic Sea during
three different seasons. The Celtic Sea is a productive, temperate sea located on the northwest
European shelf (Carr et al., 2018; Muller-Karger et al., 2005). Our three cruises transected from a
productive shelf environment out to the open ocean and our samples therefore incorporated a
range of DOC concentrations and DOM compositions from fresh DOM produced during
180 phytoplankton bloom conditions to aged DOM from deep waters (>500 m). We used Adsorptive
Cathodic Stripping Voltammetry and detected labile Fe following complexation to 1-nitroso-2-
naphthol (HNN), and calculated concentrations of free Fe (Fe^{3+}) and non-labile dissolved Fe
(DFe*) at a constant pH (pH 8) over a range of total Fe concentrations (up to 10 nmol L^{-1}). We
aimed to account for a broad range of binding strengths by using different HNN concentrations
185 (Van Den Berg et al., 1990; Hudson et al., 2003; Pižeta et al., 2015). To test scalability to

changing DOC concentration, we compared the concentrations of observed Fe species to those predicted using two sets of NICA constants previously described in the literature (Gledhill et al., 2015; Hiemstra and van Riemsdijk, 2006) and two sets more specific to DOM in our research area that we re-derived from raw titration data obtained in a previous study in our region (Avendaño et al., 2016). We identified the Fe(III) NICA constants that best fitted our observed values of Fe^{3+} and DFe^* , and used them to calculate the equilibrium speciation of Fe(III) at ambient pH and temperature in our region. We estimated the impact of Fe bound to organic matter on the truly dissolved inorganic Fe fraction (Fe^{D}) in our study region. Since Fe(III) solubility is also directly related to Fe speciation, we also examined the saturation state of Fe at ambient pH and temperature in our study region by calculating the apparent Fe(III) solubility ($\text{SFe(III)}_{\text{app}}$). We define $\text{SFe(III)}_{\text{app}}$ as the sum of aqueous inorganic Fe(III) species and Fe(III) bound to DOM formed at a free Fe (Fe^{3+}) concentration equal to the limiting solubility of Fe hydroxide ($\text{Fe(OH)}_3(\text{s})$). We discuss the observed trends in the context of observed total dissolved Fe concentrations in order to understand the relative importance of different drivers of changing Fe speciation.

3. Materials and Methods

3.1 Sampling

Samples were collected during three cruises: DY018 in autumn (November 2014), DY029 in spring (April 2015) and DY033 in summer (July 2015) in the Celtic Sea on board the RRS Discovery as part of the UK Shelf Sea Biogeochemistry programme (Birchill et al. (2017); Rusiecka et al. (2018)). Here, we examine Fe speciation at the central Celtic Sea site (CCS), a shelf edge station (CS2) and an off-shelf transect through a submarine canyon (C01-06) (Figure 1). Salinity, depth and temperature were measured using a Seabird CTD attached to a titanium rosette frame equipped with 24 x 10 L Ocean Test Equipment bottles (Birchill et al., 2017). Trace metal samples were collected following GEOTRACES protocols (Cutter et al., 2017). Samples for the determination of Fe speciation were filtered (0.2 μm cartridge filters; Sartobran-300, Sartorius) into acid-cleaned 250 ml low density polyethylene (LDPE) bottles (Nalgene) and frozen immediately (-20 °C). Samples were subsequently analyzed in a trace metal clean laboratory at GEOMAR.

3.2 Determination of dissolved Fe, dissolved organic carbon and pH

220 Samples for DFe analysis were collected after filtration through 0.2 μm cartridge filters. The samples were stored in acid cleaned LDPE bottles (Nalgene) and acidified to pH 1.7 (0.024 mol L⁻¹ HCl). Dissolved Fe concentrations were determined using flow injection with chemiluminescence detection (Birchill et al., 2017; Obata et al., 1993). The accuracy and analytical uncertainty of the method was assessed by applying the top down NordtestTM approach to the analysis of SAFe and GEOTRACES consensus materials, the combined 225 uncertainty was calculated to be 9.5 % (Worsfold et al., 2019).

Samples for the determination of DOC were collected after filtration (ashed glass fibre filters, 0.7 μm nominal pore size, Whatman), and acidified to pH 2 using hydrochloric acid. The DOC 230 samples were analyzed onshore using high temperature catalytic oxidation on a Shimadzu TOC-VCPN. Consensus reference materials (CRM; University of Miami) were used to determine accuracy and precision of analysis daily, which were both better than 4 %.

Samples for dissolved inorganic carbon (C_T) and total alkalinity (A_T) were collected via silicone 235 tubing into 250 ml borosilicate glass bottles following established protocols (Dickson, 2010). For the off-shelf transect, samples for C_T and A_T were collected only during DY018 and DY033. Each bottle was sealed shut with a greased ground glass stopper after introducing a 2.5 ml air headspace and sterilising the sample with 50 μl of saturated mercuric chloride solution. All samples were stored in the dark until analysis with VINDTA 3C instruments (Marianda, 240 Germany). The C_T and A_T measurements were calibrated using measurements of certified reference material obtained from Prof A. G. Dickson (Scripps Institution of Oceanography, USA) (Humphreys et al., 2019). The pH of our seawater samples was calculated on the IUPAC/NBS scale (pH_{NBS}) from C_T and A_T using CO2SYS (Pierrot et al., 2006). In CO2SYS, the constants describing the carbonate and sulphate equilibrium with hydrogen ions were from 245 Mehrbach et al. (1973) (refitted by Dickson and Millero (1987)) and Dickson, (1990), respectively, and the total boron concentration was estimated from salinity following Uppström,

(1974). We used the NBS pH scale because it is consistent with the speciation constants in the applied NICA-Donnan and ion pairing models.

250 3.3 Determination of iron speciation via adsorptive cathodic stripping voltammetry

Iron speciation was determined by competitive ligand equilibrium with adsorptive cathodic stripping voltammetry (CLE-AdCSV), using 1-nitroso-2-naphthol (HNN) as the added ligand (van den Berg, 1995). HNN (Sigma-Aldrich) was diluted in methanol (Fisher, HPLC grade) to make a stock solution. To clean the stock buffer solution of N-(2-Hydroxyethyl)piperazine-N'-(2-ethanesulfonic acid) (HEPES; Sigma-Aldrich), HNN was added and equilibrated with the buffer overnight. HNN and FeNN3 were subsequently removed using a pre-activated C18 SepPak column (Whatman). The pH_{NBS} of the buffer solution was adjusted to 8 prior to the titration work with ammonium hydroxide (20-22%) (Optimal, Fisher Scientific), and the pH_{NBS} of each buffered sample was determined to be between 7.9 and 8.1, with an overall average of 8.00 ± 0.08 (n=93).

Since the speciation measurements are thermodynamic, it is important that voltammetric peaks are stable and equilibrium is achieved (Laglera & Filella, 2015; Van Leeuwen & Town, 2005). In previous studies, a reaction time of > 6 h was assumed to be sufficient to reach equilibrium conditions (Avendaño et al., 2016; Boye et al., 2001; Boye et al., 2003; Gledhill & van den Berg, 1994). However, Wu and Luther (1994, 1995) waited 24 h to reach the equilibrium condition between FeL (i.e. Fe bound to natural ligand) and HNN. Here, we tested equilibration time prior to analyzing Fe speciation in our seawater samples. Our test indicated that a reaction time > 12h was needed to obtain consistent, reproducible peak heights, which we took to approximate equilibrium conditions between FeL and HNN for our method and we therefore allowed for a 16 h equilibration period.

Our speciation measurements are based on establishing an equilibrium between HNN, Fe^{3+} , binding sites (L^-) and the remaining inorganic Fe species (e.g. hydroxides) in the solution. The ratio of free to complexed species gives the side reaction coefficient (α) for the reaction (Ringbom and Still, 1972), which is also related to the conditional stability constant

($k_{FeNN_3,Fe^{3+}}^{cond}$) and the concentration of ligand not bound to Fe ($[NN']$), as shown for the formation of $FeNN_3$ in equation (3).

280

$$\frac{[FeNN_3]}{[Fe^{3+}]} = \alpha'_{FeNN_3,Fe^{3+}} = k_{FeNN_3,Fe^{3+}}^{cond} \times [NN']^3 \quad (3)$$

Species can only compete when their side-reaction coefficients are within an order of magnitude of each other, hence ligands detectable in a CLE-AdCSV titration are restricted to those with side
285 reaction coefficients (α'_{FeL}) within this “detection window” (Van Den Berg et al., 1990; Hudson et al., 2003; Kogut & Voelker, 2001). However, there may be a considerable range of ligand strengths in seawater and the use of at least two detection windows has previously been recommended to ensure the full range of ligand strengths can be accounted for (Buck et al., 2012; Pižeta et al., 2015; Sander et al., 2011). We therefore used three different total HNN
290 concentrations, $[HNN_T] = 1, 5$ and $20 \mu\text{mol L}^{-1}$.

We combined our different HNN concentrations with seven different Fe additions between 0 and 5 nmol L^{-1} at the two lower HNN concentrations (1 and $5 \mu\text{mol L}^{-1}$) and 3 concentrations ($5, 10, 15 \text{ nmol L}^{-1}$) at the highest HNN concentration ($20 \mu\text{mol L}^{-1}$) to create a matrix of 18 titration
295 points. All titration data for one sample were obtained on the same day. Our aim was to estimate the slope using our highest HNN concentration and calculate $[FeNN_3]$ according to the “overload titration” method (Kogut and Voelker, 2001). Examination of the sensitivity observed for each HNN concentration in seawater in our samples at Fe concentrations $\geq 3 \text{ nmol L}^{-1}$ showed no significant difference between sensitivity at 5 and $20 \mu\text{mol L}^{-1}$ HNN (details in supplementary
300 information, Figure S1). On the other hand, the titration point with the highest added Fe concentration (15 nmol L^{-1}) was often lower than expected, suggesting non-linearity in the titration at higher Fe concentrations, possibly caused by adsorption of the hydrophobic $FeNN_3$ complex on the walls of the voltammetric cell (Supplementary Figure S2). We thus used the data with 5 and $20 \mu\text{mol L}^{-1}$ HNN and added Fe concentrations from 3 to 10 nmol L^{-1} to calculate the
305 sensitivity of our analysis and determine the $FeNN_3$ concentration.

The concentration of HNN not complexed by Fe ($[NN']$) and the conditional stability constant ($k_{FeNN_3,Fe^{3+}}^{cond}$) of the $FeNN_3$ complex were used to derive the free Fe^{3+} concentrations in the sample at the fixed titration pH_{NBS} of 8.0 over the range of Fe concentrations according to equation (3). Since $[HNN_T] \gg [Fe]$, we assumed that $[HNN_T] = [NN']$. The cumulative random error for Fe^{3+} is largely dependent on the random error in the $FeNN_3$ concentration, as the 95 % confidence interval for the estimation of $k_{FeNN_3,Fe^{3+}}^{cond}$ was 0.2 % of the determined value (see results). We estimated an average analytical precision for our determined $FeNN_3$ concentrations of 9 % based on the mean variability of observed peak areas. However, we note this estimate does not account for errors incurred during calculation of the sensitivity, which will result in an additional random error between titrations.

The difference between the total Fe present in the solution and $[FeNN_3]$ were used to determine the non-labile dissolved Fe concentration (DFe^*):

$$DFe^* = [TFe] - [FeNN_3] \quad (4)$$

where $[TFe]$ is the concentration of total Fe (i.e. $DFe + \text{added Fe}$). DFe^* is subject to error propagation from the determinations of both $FeNN_3$ (9 %) and dissolved Fe (7 %) and thus will be subject to the combined error of 11.4 %. We therefore only report values of DFe^* where $FeNN_3$ is at least 11.4 % less than TFe .

3.4 Derivation of conditional equilibrium constant for $FeNN_3$ for application in ion pairing models for seawater

To ensure consistency between our observed $FeNN_3$ concentrations and our speciation calculations we derived an equilibrium constant valid for seawater (S=35) between pH_{NBS} 7.2-8.5 that accounts for competition between Fe and hydrogen ions for NN' .



We distinguish this constant from previously derived conditional stability constants ($\log k_{FeNN_3,Fe^{3+}}^{cond}$) by denoting it $\log k_{FeNN_3,H^+}$. We used the equilibrium constant for HNN of

10^{7.9} (NIST, Smith et al. 2004). Derivation was carried out by combining the chemical speciation program ORCHESTRA (Meeussen, 2003) with the parameter estimation software PEST (Doherty, 2019). Speciation calculations in ORCHESTRA were set up with input, chemistry and objects files as described previously (Janot et al., 2017). Further details are provided as a protocol that can be downloaded from protocols.io ([dx.doi.org/10.17504/protocols.io.brc4m2yw](https://doi.org/10.17504/protocols.io.brc4m2yw)). We used the Minteqv4 database for thermodynamic constants, which is consistent with the database used previously in visual MINTEQ (Avenidaño et al., 2016; Gledhill et al., 2015) and we also verified that calculations in ORCHESTRA and visual MINTEQ were comparable. The control and input files for PEST (see [dx.doi.org/10.17504/protocols.io.brc4m2yw](https://doi.org/10.17504/protocols.io.brc4m2yw)) were written in a text editor and the two software programs combined via a dedicated windows command line function. For the derivation of $\log k_{FeNN_3,H^+}$ we specified an initial estimate of 31, with an allowed range of 28 to 32. Parameter derivation is performed by calculation of the FeNN₃ concentration in ORCHESTRA for each measurement, which is then passed to PEST and compared to the observed values. PEST provides a new value for $\log k_{FeNN_3,H^+}$, which is then passed back to ORCHESTRA for a fresh calculation of FeNN₃. The procedure is iterated to minimize the residuals between observed and calculated FeNN₃ calculations via the Levenberg-Marquardt algorithm. The PEST output comprises a value for $\log k_{FeNN_3,H^+}$ with 95% confidence intervals, together with a full record of the optimization in the output file. Consistency was then further assessed by comparison between observed and calculated FeNN₃ and Fe³⁺ in UV irradiated seawater as a function of HNN concentration, within the HNN concentration range applied in this study.

3.4 Assessment of relationship between observed and calculated concentrations of iron species to DOC concentrations assuming binding sites behave according to the NICA-Donnan model.

The NICA-Donnan model was used to calculate the speciation of Fe at equilibrium for each titration point at pH_{NBS} 8.0, via speciation calculation tool ORCHESTRA (Meeussen, 2003). We tested the assumption that one set of NICA-Donnan parameters could describe variability in [FeNN₃] and [Fe³⁺] by adding the “FA” NICA-Donnan adsorption model to the dissolved ion pairing model used for the derivation of $\log k_{FeNN_3,H^+}$ described in section 3.3. Marine DOM was thus considered analogous to terrestrial and freshwater DOM (Gledhill et al., 2015; Laglera

& Van Den Berg, 2009; Lodeiro et al., 2020). The applied NICA model assumes a continuous
 370 Sips bimodal distribution of binding sites. The distribution of the affinities of the two groups of
 binding sites (Denoted (1): Carboxylic-type groups, and (2): Phenolic-type groups) are described
 by three constants per binding site group: the width of the binding site distribution (p_1 and p_2),
 NICA affinity constant ($\log K_{Me1}$ and $\log K_{Me2}$ for a metal cation or $\log K_{H1}$ and $\log K_{H2}$ for the
 protonation constants) which represents the median of the distribution, and non-ideality constant
 375 which represents non-ideal behavior of ion adsorption (n_{Me1} , n_{Me2} , n_{H1} , n_{H2}), with $n = 1$
 representing ideal behavior (Kinniburgh et al., 1999). The binding of a metal by marine DOM,
 Q_{Me} is then described with reference to proton binding by marine DOM according to the
 following equation:

$$\begin{aligned}
 380 \quad Q_{Me} = & Q_{max1,T} \frac{n_{Me,1}}{n_{H1}} \cdot \frac{(K_{Me,1} \cdot C_{Me})^{n_{Me,1}}}{(K_{H,1} \cdot C_H)^{n_{H,1}} + (K_{Me,1} \cdot C_{Me})^{n_{Me,1}}} \cdot \frac{\{(K_{H,1} \cdot C_H)^{n_{H,1}} + (K_{Me,1} \cdot C_{Me})^{n_{Me,1}}\}^{p_1}}{1 + \{(K_{H,1} \cdot C_H)^{n_{H,1}} + (K_{Me,1} \cdot C_{Me})^{n_{Me,1}}\}^{p_1}} + \\
 & Q_{max2,T} \frac{n_{Me,2}}{n_{H2}} \cdot \frac{(K_{Me,2} \cdot C_{Me})^{n_{Me,2}}}{(K_{H,2} \cdot C_H)^{n_{H,2}} + (K_{Me,2} \cdot C_{Me})^{n_{Me,2}}} \cdot \frac{\{(K_{H,2} \cdot C_H)^{n_{H,2}} + (K_{Me,2} \cdot C_{Me})^{n_{Me,2}}\}^{p_2}}{1 + \{(K_{H,2} \cdot C_H)^{n_{H,2}} + (K_{Me,2} \cdot C_{Me})^{n_{Me,2}}\}^{p_2}} \quad (6)
 \end{aligned}$$

where $Q_{max1,T}$, $Q_{max2,T}$ refer to the total number of proton binding sites per binding site type,
 and C_H and C_{Me} are the concentrations of protons and metal, respectively.

385

In the NICA-Donnan model, electrostatic interactions are described by the Donnan component of
 the model which is based on the Boltzmann equation (Benedetti et al., 1996). However, at the
 ionic strength of seawater the apparent Donnan volume becomes very small and concentrations
 of metals electrostatically associated with DOM become negligible (Lodeiro et al., 2020;
 390 Pinheiro et al., 2021).

In this study, we used two previously published sets of NICA constants and two new NICA
 parameter sets (Table 1). The previously published sets were derived from surface waters
 collected in the Sargasso Sea (Set A: Hiemstra and van Riemsdijk, 2006) and surface waters
 395 obtained from an estuarine system on the English south coast (Set B: Gledhill et al. 2015), whilst
 the new parameter sets C and D were re-derived from surface waters in the Northwest European
 Shelf Sea based on titration data obtained in Celtic Sea samples first reported in Avendaño et al.
 (2016). We re-derived the set C and D values because the original reported values were

empirically estimated using a $\log k_{FeNN_3,H^+}$ of 32.5, which was considerably higher than the
400 value we derived in this study (see results). We used PEST-ORCHESTRA to re-derive the NICA
constants following a similar procedure used for the derivation of $\log k_{FeNN_3,H^+}$. Since this work
was focused on the Celtic Sea, we only used the titration data obtained from Celtic Sea samples
in this derivation (samples collected at stations 1, 3, 4, 5, 6, 18, 19, 20 from Avendaño et al.
(2016)). We provide the raw titration data, required input files and a description of the protocol
405 used in this derivation on protocols.io (dx.doi.org/10.17504/protocols.io.brc4m2yw). We
followed the PEST-ORCHESTRA approach that was first used to derive NICA constants for Cd
and Zn binding to Laurentian fulvic acid by Janot et al. (2017). Typically, both equilibrium
constants and non-ideality constants are derived from experimental data. However, we found
during preliminary derivations that since titrations were undertaken at only three pH_{NBS} values
410 (7.2, 7.6, 8) and encompassed a relatively narrow pH range, data from Avendaño et al. (2016)
were not sufficiently well constrained in pH space to reproducibly derive all four parameters. We
therefore fixed $n_{Fe(III)1}$ and used the relationship between n_1 and n_2 from Milne et al. (2003)
($n_2 = 0.76 \times n_1$) to calculate $n_{Fe(III)2}$. We then estimated $\log K_{Fe(III)1}$, $\log K_{Fe(III)2}$ using initial
guesses of 3 and 9, and ranges of 2 to 4 and 8 to 10, respectively. Generic parameters from Milne
415 et al. (2003), (2001) were used to describe binding of proton and major cations (H^+ , Ca^{2+} , Mg^{2+} ,
 Sr^{2+}) to be consistent with parameter sets A and B.

To investigate goodness of fit at different ambient DOC concentrations, we compared our
observed $FeNN_3$ concentrations with $FeNN_3$ concentrations calculated in ORCHESTRA. We
420 then compared Fe^{3+} calculated from observations using equation (3) with those calculated in
ORCHESTRA and observed versus calculated D_{Fe^*} calculated using equation (4). For
speciation calculations, pH was set to the analysis pH_{NBS} ($= 8.00 \pm 0.08$).

3.5 Prediction of apparent Fe(III) solubility and inorganic Fe concentrations at ambient pH and 425 temperature in our study region

We predicted Fe speciation in our study area at ambient pH and temperature using the NICA
constants with the best fit to our observed titration data. To calculate $S_{Fe(III)app}$ we set our total
Fe(III) concentration to 10 nmol L^{-1} and allowed for the formation of $Fe(OH)_3(s)$ (ferrihydrite)

430 within ORCHESTRA. We use a solubility product of $\log K_s = 3.2$, derived from (Liu and
Millero, 1999) to determine iron solubility according to equation (7).

$$*K_{SO} = [Fe^{3+}] \div [H^+]^3 = 10^{3.2}, \Delta H_r = -100.4 \text{ kJ mol}^{-1} \quad (7)$$

435 We therefore consider organically bound Fe as soluble, but freshly precipitated $Fe(OH)_3(s)$ as
insoluble. We compare our $SFe(III)_{app}$ with observed dissolved Fe concentrations. However,
given the potential size of both freshly formed $Fe(OH)_3(s)$ (defined in Liu and Millero (1999)
as $>0.02 \mu m$) and organic matter (determined in the $<0.7 \mu m$ fraction), the Fe associated with
both DOM and $Fe(OH)_3(s)$ may both be colloidal in nature (>0.02 but $<0.2 \mu m$) and this should
440 be kept in mind when comparing the absolute values.

We calculated the sum of soluble inorganic species and express these concentrations as $pFe(III)'$
using:

$$445 \quad pFe(III)' = -\text{Log} ([FeOH^{2+}] + [Fe(OH)_2^+] + [Fe(OH)_3] + [Fe(OH)_4^-]) \quad (8)$$

In these calculations, we set the total Fe concentration to be equal to the determined DFe
concentration, but $Fe(OH)_3(s)$ was also allowed to form to account for possible formation of
insoluble iron hydroxides when Fe^{3+} becomes oversaturated, according to equation (7).

450

4. Results and Discussion

4.1 Establishing consistency between observations and calculations in the absence of organic matter.

455 An understanding of how pH and temperature might influence trace element speciation at
equilibrium can be obtained via iterative algorithms based on thermodynamic principles using
sets of thermodynamic constants valid for the physico-chemical conditions to be explored in the
study. We applied “off the shelf” ion pairing software packages in our study that incorporate
ionic strength corrections based on the extended Debye-Hückel equation, but we highlight this is
460 not fully optimal and warn that absolute values predicted via our speciation calculations will be

affected by systematic bias as a result of overestimation of activities. The impact of the ion pairing approach is illustrated by an approximate 15% underestimation in ionic strength in our calculation ($I=0.6$ M), which is consistent with previous estimates of the error introduced by application of the Debye-Hückel equation (Stockdale et al., 2016). Nevertheless, valuable
465 information – with respect to the extent that changes in physico-chemical properties such as pH and temperature may have on metal speciation – can be obtained if a system can be calibrated such that its observed and calculated values are consistent for a given critical species. In our study, we used a value for $\log k_{FeNN_3,H^+}$ within an ion pairing model, which would account for competition between NN^- , H^+ , Fe^{3+} and OH^- at the ionic strengths and pH relevant to our study.
470 In previous work, a first attempt at such a system was made by manually changing constants to obtain an empirical estimate for $\log k_{FeNN_3,H^+}$ (Avendaño et al., 2016). In this study, we sought to improve on this by first calibrating $\log k_{FeNN_3,H^+}$. We particularly focused on establishing consistency between determined and calculated Fe^{3+} and $FeNN_3$ concentrations, since $FeNN_3$ is the measured species from titrations and Fe^{3+} is the Fe species that reacts with the added ligand,
475 hydroxide ion and natural organic matter.

Estimation of $\log k_{FeNN_3,H^+}$ using the parameter estimation software package PEST (Doherty, 2019) in combination with the ion pair speciation program ORCHESTRA (Meeussen, 2003) resulted in a $\log k_{FeNN_3,H^+}$ of 29.5 ± 0.1 . With this value, the correlation coefficient between
480 observed and calculated $\log[FeNN_3]$ was 0.962 with a root mean squared error (RMSE) of 1.12 $nmol\ L^{-1}$ over the pH_{NBS} range 7.2-8.5 and at an HNN concentration of $2\ \mu mol\ L^{-1}$. Predicted Fe^{3+} concentrations (Fe^{3+}_{calc}) correlated with Fe^{3+} calculated from the observed $FeNN_3$ concentrations ($Fe^{3+}_{titration}$) ($\log[Fe^{3+}]_{calc} = 0.95 \times \log[Fe^{3+}]_{titration} - 0.83$, $r^2 = 0.97$, $n=456$) (Figure 2a). The modelled distribution of the relative proportion of Fe present as $FeNN_3$ as a function of
485 pH suggests that $FeNN_3$ will be the dominant species between pH_{NBS} 7 and 8, with a maximum response at pH_{NBS} 7 (Figure 2b), which is consistent with the relationship between pH and the voltammetric response for $FeNN_3$ previously reported by van den Berg (1991). However, our derived value of 29.5 for $\log k_{FeNN_3,H^+}$ is three orders of magnitude lower than the empirical estimate of 32.5 given by Avendaño et al. (2016). Further comparison with literature values
490 showed that our calculated conditional stability constant at pH_{NBS} 8 is within the reported range after calibration against hydroxide and EDTA but lower than obtained at pH_{NBS} 6.9

(Supplementary Table 1). The difference between the calibrated constants could be explained by the ionic strength corrections applied during the calculations, the choice of conditional constants for Fe binding to EDTA, and the applied inorganic side reaction coefficient for Fe (Laglera et al., 495 2011).

We next examined the relationship between calculated and determined FeNN_3 and Fe^{3+} concentrations using the derived $\log k_{\text{FeNN}_3, \text{H}^+}$ over the range of HNN concentrations (1, 5 and 20 $\mu\text{mol L}^{-1}$) employed in this study at pH_{NBS} 8.0 using the ‘overload titration’ method. We 500 obtained a linear relationship between observed and calculated $[\text{Fe}^{3+}]$ ($\log[\text{Fe}^{3+}]_{\text{calc}} = 1.07 \pm 0.03 \times \log[\text{Fe}^{3+}]_{\text{titration}} + 8.7 \times 10^{-20} \pm 6.5 \times 10^{-20}$, $r^2 = 0.93$, $n = 98$, Figure 2c). The positive intercept implies a slight systematic overestimate of FeNN_3 by the ion pairing model, which is supported by the relationship between the proportion of Fe bound to FeNN_3 and the HNN concentration (Figure 2d). The observed proportion of Fe(III) that was detected as FeNN_3 at both 1 and 5 $\mu\text{mol L}^{-1}$ 505 HNN was thus slightly lower (by an average of 10 and 15 % respectively) than predicted by the ion pairing model. Our calculated side reaction coefficients were $\log \alpha'_{\text{FeNN}_3, \text{Fe}^{3+}} = 9.1, 11.2$ and 13 for 1, 5 and 20 $\mu\text{mol L}^{-1}$ HNN, respectively. These values compared to a $\log \alpha'_{\text{Fe}}$ of 8.95 calculated by the ion pairing model at pH_{NBS} 8.0. The similarity between $\log \alpha'_{\text{FeNN}_3, \text{Fe}^{3+}}$ and $\log \alpha'_{\text{Fe}}$ at an HNN concentration of 1 $\mu\text{mol L}^{-1}$ means that hydroxide ions will compete with 510 HNN at our lowest HNN concentration (Figure 2c). Given the low solubility of Fe hydroxides (at pH_{NBS} 8.0 and 293 K, $\text{Fe}(\text{OH})_3(\text{s})$ is predicted to form at an $[\text{Fe}^{3+}]$ concentration of 7.58×10^{-20} mol L^{-1} , equivalent to $\text{pFe}(\text{III})' = 10.2$), the relatively high proportion of Fe^{3+} (maximum calculated Fe^{3+} in UV irradiated seawater = 5.7×10^{-18} mol L^{-1}) should theoretically result in formation of $\text{Fe}(\text{OH})_3(\text{s})$ at both 1 and 5 $\mu\text{mol L}^{-1}$ HNN concentrations. Nevertheless, the linear 515 relationship between observed and calculated Fe^{3+} suggests that $\text{Fe}(\text{OH})_3(\text{s})$ formation did not impact on the determination of FeNN_3 , possibly because we always added HNN prior to addition of Fe. The binding of Fe to HNN therefore occurred more quickly than formation of $\text{Fe}(\text{OH})_3(\text{s})$. If we assume no formation of $\text{Fe}(\text{OH})_3(\text{s})$ occurred, then Fe^{3+} concentrations are consistent over the range of pH and HNN values examined here.

520 We concluded that our experiment - speciation calculation framework was adequately consistent within the time frame of our titration experiments. However, we caution that our experiments are

likely not at true equilibrium, and while it was not detectable over the <24-hour equilibration period of our titrations, we cannot completely rule out formation of Fe(OH)₃(s). Although our
525 calculations simplify the complex kinetic and thermodynamic processes that influence chemical Fe speciation in aqueous solutions, we argue that they are sufficiently consistent to be used to investigate the relationship between DOC concentration and Fe speciation predicted by the NICA-Donnan model.

530 As a final step in the development of our experimental framework for examining the relationship between DOC concentrations and the fit of observed Fe speciation to different sets of NICA parameters, we re-derived the NICA constants from Avendaño et al. (2016). We carried out this re-derivation to improve upon the empirical nature of the original estimates and to account for the difference in $\log k_{FeNN3,H+}$ used to generate the estimates for the NICA affinity constants
535 reported by Avendaño et al. (2016). When fitting for four parameters ($n_{Fe(III)1}$, $n_{Fe(III)2}$, $\log K_{Fe(III)1}$, $\log K_{Fe(III)2}$) we found that repeated estimations ($n > 3$) using the same initial arbitrary parameter values did not produce reproducible results, likely as a result of overfitting the data set. The value of n_i and its relationship to n_H as described in equation (6) have been related to reaction stoichiometry between H⁺ and the metal ion (Hiemstra and van Riemsdijk,
540 2006), thus determination of n_i requires experimental data with sufficient density and range in pH space. Unfortunately, we found that this criterion was not satisfied by the data of Avendaño et al. (2016), since titrations at only 3 pH values within a relatively restricted range (less than one pH unit) were undertaken. We therefore initially set the value for $n_{Fe(III)1}$ to 0.31 based on previously reported values available for marine organic matter (Avendaño et al., 2016; Gledhill
545 et al., 2015; Hiemstra and van Riemsdijk, 2006). The value of $n_{Fe(III)2}$ was calculated using the formula $n_2 = 0.76 \times n_1$ which has previously been shown to describe the covariance between n_1 and n_2 observed for multiple cations (Milne et al., 2003). Our re-derived NICA affinity constants (set C) are presented in Table 1 along with a further two sets of constants (sets A and B) taken from the literature (Gledhill et al., 2015; Hiemstra and van Riemsdijk, 2006) that we use directly.
550 As expected, the combination of fixing n_i , the mathematical rederivation and the change in $\log k_{FeNN3,H+}$, resulted in differences in the derived $\log K_{Fe(III)1}$ and $\log K_{Fe(III)2}$ used in this study compared to the values empirically estimated (0.26, 3.6, 0.23 and 8.3 for $n_{Fe(III)1}$,

$\log K_{Fe(III)1}$, $n_{Fe(III)2}$, $\log K_{Fe(III)2}$ respectively) by Avendaño et al. (2016). We further examined the impact of n_i by increasing the value of n_1 and n_2 to consider the possibility that marine DOM is more ideal (i.e. less heterogeneous) than typically observed for terrestrial organic matter (set D) (Lodeiro et al., 2020). As well as influencing the effective competition between the metal and protons (Milne et al., 2003), the non-ideality constant influences the relationship between the free metal ion concentration and the total dissolved metal concentration (also termed the concentration dependency, Milne et al. 2003). Incorporation of heterogeneity results in an exponential increase in Fe^{3+} as DFe concentrations increase, which arises because stronger binding sites in the distribution are occupied first. Higher, more ideal, values of n_i result in a shallower exponential curve for the relationship between Fe^{3+} and DFe concentrations.

Table 1. Four sets of constants for Fe(III) binding to the two dissolved organic matter binding site types of the NICA-Donnan model. Parameter sets A and B were taken from the literature, Hiemstra and van Riemsdijk (2006) and Gledhill et al. (2015), respectively. Parameter sets C and D were re-derived for this study based on raw titration data obtained in Celtic Sea samples previously reported in Avendaño et al. (2016). We fixed the non-ideal constants ($n_{Fe(III)}$) to derive the binding affinity ($\log K_{Fe(III)}$) for both parameter sets C and D. The goodness of fit is indicated as root mean square error (RMSE).

Fe(III) NICA constants	set A	set B	set C	set D
FA1: Carboxylic-type groups				
$\log K_{Fe(III)1}$	2.8	3.6	2.81±0.36	3.16±0.001
$n_{Fe(III)1}$	0.36	0.3	0.31	0.4
FA2: Phenolic-type groups				
$\log K_{Fe(III)2}$	8.3	11.2	9.04±0.01	9.80±0.01
$n_{Fe(III)2}$	0.23	0.15	0.24	0.3

RMSE for parameters rederived in this study	NA	0.7908	0.2149
---	----	--------	--------

4.2 Influence of dissolved organic carbon concentration on determined and calculated Fe speciation at constant pH

575

In this work, we analyzed 106 samples from three cruises undertaken in November (DY018, 47 samples), April (DY029, 34 samples) and July (DY033, 28 samples) by CLE-AdCSV and present raw titration data in the SI (Supplementary Figure S2). We first compared FeNN₃ concentrations calculated with the NICA-Donnan model using parameter sets A-D with the observed FeNN₃ concentrations for the whole data set (Table 2, Supplementary Figure S3). Simulated FeNN₃ using parameter set B systematically underestimated the observed FeNN₃ concentrations, resulting in a larger RMSE in comparison to sets A, C and D (Table 2).

580

Parameter set B thus overestimated the binding strength of organic matter in our study region. The stronger binding represented by parameter set B could reflect the estuarine nature of the samples used for the parameter estimation, which might be more strongly influenced by terrestrial organic matter. However, we caution that the data set used for the estimation in Gledhill et al. (2015) was also limited and the authors of that study emphasized that it was intended as a proof of concept.

585

590 Table 2. Relationships between calculated (y) and observed (x) FeNN₃ concentrations obtained using four sets of NICA constants. Sets A and B and are taken from the literature, Hiemstra and van Riemsdijk (2006) and Gledhill et al. (2015), respectively. Sets C and D were re-derived for this study based on titrations data taken from Avendaño et al. (2016). The number of observations was 643. The goodness of fit is indicated as root mean square error (RMSE).

595

Fe(III) NICA constants	set A	set B	set C	set D
Linear equation	$y=1.03x+0.36$	$y=8.05x-0.79$	$y=1.03x+0.50$	$y=1.03x+0.39$
r^2	0.85	0.78	0.84	0.85

RMSE (nmol L ⁻¹)	0.95	1.52	0.89	0.98
------------------------------	------	------	------	------

FeNN₃ is a dominant species at 5 and 20 μmol L⁻¹ HNN in our titration experiments, and variability in less abundant species might be expected to be more sensitive to changes in binding site concentrations and better highlight systematic bias with respect to DOC concentrations.

600 Therefore, we next compared the relationship between [Fe³⁺]_{titration} and total Fe with calculated values for Fe³⁺ obtained from combining the ion-pairing and NICA model ([Fe³⁺]_{NICA}) using our four sets of NICA constants for samples binned into three different DOC concentrations: 45-55, 55-65, and >65 μmol L⁻¹ (Figure 3). The DOC bins broadly align with concentrations typically observed for semi-refractory, semi-labile and labile DOC respectively (Hansell, 2013), although
605 the division between the different DOC fractions is likely less well defined than implied here. Figure 3 shows that the relationship between [Fe³⁺]_{titration} and total Fe was quite well described by A, C and D, but not well described by parameter set B, although some differences between Fe³⁺ at 1 μmol L⁻¹ HNN at low total Fe concentrations was evident for all sets at DOC concentrations > 55 μmol L⁻¹. Results of correlation between [Fe³⁺]_{titration} and [Fe³⁺]_{NICA} are
610 given in Table 3. Calculated [Fe³⁺]_{NICA} using parameter sets A, C and D again showed better agreement with [Fe³⁺]_{titration} (Table 3) than parameter set B. Combining information from intercept, slope and r² and Akaike Information Criteria (AIC), A and D were found to be a better fit to the data than C.

615 We noted that goodness-of-fit of [Fe³⁺]_{NICA} to [Fe³⁺]_{titration} tended to decrease with increasing DOC concentration (Table 3). We therefore further examined the scenario that binding sites did not scale with DOC concentration by calculating the Fe speciation using parameter set D and fixing the DOC concentration to the lowest value observed in our study (43.7 μmol L⁻¹). We found similar goodness-of-fit results for this fixed-DOC scenario (D2) across the whole range of
620 DOC concentrations observed in our study, suggesting that binding sites are not necessarily more abundant as DOC concentration increases.

Table 3. Correlations of log[Fe³⁺]_{titration} (x) observed in titrations undertaken at different HNN concentrations with log[Fe³⁺]_{NICA} (y) calculated using a combined ion-pair/NICA-Donnan
625 model. Sets A and B and are taken from the literature, Hiemstra and van Riemsdijk (2006) and

Gledhill et al. (2015), respectively. Sets C and D were rederived for this study based on titration data taken from Avendaño et al. (2016). The D2 scenario used parameter set D but assumed a constant DOC concentration of $43.7 \mu\text{mol L}^{-1}$.

DOC concentration ($\mu\text{mol L}^{-1}$)	NICA parameter set	Intercept	Slope	R ²	AIC
45-55 (n=612)	A	-1.21±0.16	0.93±0.01	0.95	-55
	B	-10.77±0.64	0.50±0.03	0.27	1655
	C	-2.67±0.18	0.85±0.01	0.93	116
	D	-1.24±0.16	0.93±0.01	0.96	-80
	D2	-1.05±0.16	0.93±0.01	0.96	-89
55-65 (n=643)	A	-1.34±0.14	0.92±0.01	0.96	-138
	B	-9.96±0.76	0.55±0.03	0.23	2008
	C	-2.83±0.2	0.85±0.01	0.91	289
	D	-1.38±0.14	0.92±0.01	0.97	-202
	D2	-1.04±0.13	0.93±0.01	0.97	-249
65-200 (n=234)	A	-2.06±0.32	0.89±0.02	0.92	117
	B	-13.1±1.68	0.43±0.09	0.09	881
	C	-4.2±0.48	0.79±0.03	0.80	303
	D	-2.04±0.29	0.89±0.01	0.94	62
	D2	-1.18±0.25	0.92±0.01	0.96	-16

630

For our final assessment employing our titration data, we examined the relationship between the non-labile Fe concentrations (DFe^*) and $[\text{Fe}^{3+}]_{\text{titration}}$ observed in our titrations and compared the relationship to values calculated using the NICA model. For both titration data and simulated results using the NICA-Donnan model, DFe^* was calculated using equation (4); at $1 \mu\text{mol L}^{-1}$ HNN, this fraction therefore incorporates a portion of the Fe bound to hydroxides. Figure 4 shows the relationship between DFe^* and Fe^{3+} of measured ($\text{DFe}^*_{\text{titration}}$) and calculated data ($\text{DFe}^*_{\text{NICA}}$), binned according to DOC concentration. We observed larger scatter in the calculations of DFe^* at each HNN concentration and weak correlations ($r^2 < 0.2$, data not shown)

635

between $DFe^*_{\text{titration}}$ and DFe^*_{NICA} , which likely reflects increased error propagation and the
640 limited range of DFe^* values that can be observed using AdCSV. However, for the most part,
observed $DFe^*_{\text{titration}}$ fell between calculated values obtained for parameter set B and those
obtained in the absence of organic matter (no DOM) and overlapped with parameter sets A, C
and D. The overload titration method assumes that DFe^* will be negligible at $20 \mu\text{mol L}^{-1}$ HNN,
and indeed we rarely observed DFe^* values greater than 11 % of total Fe at this HNN
645 concentration. Data points where DFe^* was detected at $20 \mu\text{mol L}^{-1}$ HNN were scattered through
the data set and thus result from random error rather than systematic offsets associated with
individual samples. Furthermore, we note that at $5 \mu\text{mol L}^{-1}$ HNN, concentrations of $[\text{FeNN}_3]_{\text{calc}}$
were overestimated in our UV seawater experiments (Figure 2d), which could contribute further
to discrepancies between $DFe^*_{\text{titration}}$ and DFe^*_{NICA} . The analytical limitations of CLE-AdCSV
650 should also be considered here, since its results are known to be influenced by the estimation of
sensitivity, lack of equilibrium conditions, and the number and distribution of titration points
(Gledhill and Gerringa, 2017; Hudson et al., 2003; Pižeta et al., 2015; Town and Filella, 2000).
In particular, the calculation of DFe^* is sensitive to bias in estimation of the slope (Hudson et al.,
2003), and the ability to detect significant concentrations of DFe^* is strongly influenced by the
655 sensitivity of the method. In our case, we note that HNN is one of the least sensitive ligands that
can be used to detect Fe by CLE-AdCSV (Ardiningsih et al., 2021), although it has the
advantage that it forms one dominant species (Waska et al., 2016), which simplifies application
over a range of added ligand concentrations (Abualhaija and van den Berg, 2014). The FeNN_3
complex can also be detected over a relatively wide pH range (van den Berg, 1991), allowing
660 speciation analysis to be applied to the ligand over a range of pH values (Avendaño et al., 2016;
Gledhill et al., 2015).

Taken together, the calculated $[\text{Fe}^{3+}]_{\text{NICA}}$ values in our titrations suggest parameter sets A and D
provide the best approximations of $[\text{Fe}^{3+}]_{\text{titration}}$. Examination of DFe^* suggests that NICA
665 parameters A, C and D predict DFe^* within the range of observed values. Considering NICA
sets A and D, binning the data into three different DOC concentrations showed that goodness of
fit decreased slightly with increasing DOC concentration (Table 3). The increase in negative
intercept with increased DOC concentration suggests that this was because the NICA model
slightly overestimated Fe binding to DOM at higher DOC concentrations, and this effect was

670 largely eliminated by assuming a constant DOC concentration of $43.7 \mu\text{mol L}^{-1}$ with parameter
set D. The overestimation of the impact of increasing DOC concentrations could point to dilution
of the Fe-binding functional groups by input of fresh DOM with a lower binding site density.
Since the main source of fresh DOC in our study area is phytoplankton (Carr et al., 2018; Davis
et al., 2018), this would imply that the overall binding affinity of DOM produced by
675 phytoplankton is lower than the aged DOM pool. However, such a trend could also be observed
if the use of generic NICA constants from (Milne et al., 2003) results in an overestimation of
binding site heterogeneity for marine DOM. There is a paucity of data investigating the acid-base
binding characteristics of marine DOM, so we recommend further investigation of total binding
site concentrations and binding site heterogeneity as a function of DOM mass (Lodeiro et al.,
680 2020), particularly with respect to the changes in DOM composition as a function of
productivity. Furthermore, we recommend that alternative experimental designs for titrations are
explored for their ability to derive intrinsic, rather than conditional, metal binding constants (e.g.
titrations over a wider range of pH values (Avenidaño et al., 2016; Gledhill et al., 2015)).

685 **4.3 Prediction of Fe(III) speciation in the Celtic Sea using ambient pH and dissolved organic carbon concentrations**

4.3.1 The combined impact of variability in pH and DOC concentration and choice of NICA constants on calculated Fe speciation.

690 For a heterogeneous group of binding sites, $D\text{Fe}$, pH, and DOC all influence $\text{pFe(III)}'$. We
illustrate the relative importance of the key parameters for driving variability in $\text{pFe(III)}'$ with
model experiments (Figure 5a and b). We calculated $\text{pFe(III)}'$ with three scenarios based on the
minimum and maximum observed values for pH and DOC we encountered in our study area: i)
 $\text{pH}_{\text{NBS}} = 8.1$, $\text{DOC} = 45 \mu\text{mol L}^{-1}$ ii) $\text{pH}_{\text{NBS}} = 8.3$, $\text{DOC} = 45 \mu\text{mol L}^{-1}$ and iii) $\text{pH}_{\text{NBS}} = 8.3$, DOC
695 $= 150 \mu\text{mol L}^{-1}$. We compare these scenarios with values calculated using ambient pH and DOC,
without considering the formation of $\text{Fe(OH)}_3(\text{s})$. The shape of the $\text{pFe(III)}'$ - $D\text{Fe}$ curve is
primarily driven by the change in $D\text{Fe}$ concentration. The different scenarios show that the DOC
range encountered in our study area has a greater potential impact on $\text{pFe(III)}'$ than pH does,
especially for parameter set D, with which scenarios (i) and (ii) overlap. The low impact of pH

700 arises because pH did not vary greatly in the study region (range of ~0.2) and because the lower heterogeneity described by parameter set D reduced the impact of pH.

We compared the data points and the solid curve in Figure 5 (a) and (b) and observed a decrease in $p\text{Fe(III)}'$ of approximately 1 and 0.5 log units at our lowest DFe concentrations and 2 and 1 log units at our highest DOC concentrations for parameter sets A and D, respectively. These values provide an estimate of the likely error in $p\text{Fe(III)}'$ introduced by scaling to DOC and, not surprisingly, show that the greatest impact will occur at the highest DOC concentrations. The differences between the magnitude of the estimates for sets A and D relate to the degree of heterogeneity, as described by the non-ideality constant, with set D describing a less heterogeneous distribution of binding sites than set A.

710

4.3.2 Impact of pH, DOC and temperature on apparent Fe(III) solubility in the Celtic Sea

Fe(III) solubility strongly influences the overall Fe inventory in the ocean (Johnson et al., 1997) and in the absence of ligands the oceanic DFe inventory would be significantly lower (Hunter and Boyd, 2007; Liu and Millero, 2002). Previous work has suggested that the ocean is saturated with respect to Fe(III) hydroxide (Byrne & Kester, 1976; Kuma et al., 1996, 1998, 2003). However, CLE-AdCSV determinations suggested that ligand concentrations are in excess of DFe, which implies that Fe(III) hydroxide might be undersaturated at the pH of the measurement (Caprara et al., 2016). The saturation state of Fe in the ocean is thus subject to some uncertainty. Furthermore, the interplay between scavenging and solubility is poorly constrained (Tagliabue et al., 2016), and the potential impact of changes in ambient seawater pH on Fe solubility has rarely been considered (Millero et al., 2009; Ye et al., 2020).

Our calculations of $[\text{Fe}^{3+}]$ at the ambient pH and DOC concentrations described above resulted in a maximum value of $4.5 \times 10^{-19} \text{ nmol L}^{-1}$ for both parameter sets A and D, obtained at the highest DFe concentration of 1.9 nmol L^{-1} (Figure 5, a and b). At $\text{pH}_{\text{NBS}} 8.0$ and 20°C , our ion pairing model predicts formation of $\text{Fe}(\text{OH})_3(\text{s})$ at an Fe^{3+} concentration of $7.58 \times 10^{-20} \text{ mol L}^{-1}$. Therefore our predicted Fe^{3+} concentrations were oversaturated with respect to $\text{Fe}(\text{OH})_3(\text{s})$. We therefore used iterative speciation calculations to investigate the potential interaction between Fe(III) solubility, temperature, pH and Fe binding to DOM in our study area. We calculated apparent

730

Fe(III) solubility ($S_{Fe(III)_{app}}$) by setting the total Fe(III) concentrations to 10 nmol L^{-1} for all samples in the model, thereby ensuring formation of the insoluble $Fe(OH)_3(s)$ species. $S_{Fe(III)_{app}}$ was then expressed as the sum of the concentrations of aqueous inorganic Fe(III) species and Fe(III) bound to DOM.

735

Figure 5 (c) and (d) shows the variation of calculated $S_{Fe(III)_{app}}$ plotted as a function of temperature for parameter sets A and D respectively. Trends for $S_{Fe(III)_{app}}$ for both parameter sets were similar and the highest $S_{Fe(III)_{app}}$ was observed at maximum DOC concentrations. Whilst DOC was an important influence on $S_{Fe(III)_{app}}$, decreased temperature and pH also both lead to increasing $S_{Fe(III)_{app}}$ (Figure 5, c and d). We assessed the relative importance of pH and temperature by calculating $S_{Fe(III)_{app}}$ using the same scenarios described for calculation of $pFe(III)'$ (section 4.3.2). We observed that pH had a greater impact on $S_{Fe(III)_{app}}$ than on $pFe(III)'$. However, in the scenario where Fe binding does scale with DOC concentration, DOC was more important than pH for our study area.

745

Comparisons between NICA parameter sets A and D showed that $S_{Fe(III)_{app}}$ was 0.05 nmol L^{-1} higher for parameter set A than for parameter set D at our lowest DOC concentration ($43.7 \text{ } \mu\text{mol L}^{-1}$) and 0.2 nmol L^{-1} higher at our highest DOC concentration ($111 \text{ } \mu\text{mol L}^{-1}$) (Figure 5, c and d). The difference was driven by changes in the affinity constant and the relative non-ideality of the binding sites, which effectively results in a lower binding affinity for parameter set D in comparison to parameter set A.

750

Both parameter sets predict maximum $S_{Fe(III)_{app}}$ values (1.2 and 1.1 nmol L^{-1}) that are lower than the determined maximum DFe concentrations (1.9 nmol L^{-1}). We emphasize that absolute values have to be compared with caution because of systematic errors in the calculations from e.g. ionic strength corrections. Here, we also need to consider the influence of physical size and filter size cut-off, since solubility was determined with $0.02 \text{ } \mu\text{m}$ filter cut off, Fe binding characteristics with a $0.2 \text{ } \mu\text{m}$ filter cut off range and DOC concentrations used in this study were determined in the $<0.7 \text{ } \mu\text{m}$ fraction. We note that fresh Fe hydroxide nanoparticles can be as small as 2-3 nm (Cismasu et al., 2011; Janney et al., 2000) and would thus be classed as dissolved when a $0.02 \text{ } \mu\text{m}$ filter cut off is employed. In addition, scavenging processes in which

760

DFe is potentially reversibly adsorbed onto solid phases present in the water column are thought to be an important influence on DFe concentrations (Achterberg et al., 2018; Fitzsimmons et al., 2017) but are not considered in our approach. It is therefore difficult to precisely map our
765 predicted $\text{SFe(III)}_{\text{app}}$ onto DFe concentrations. Nevertheless, we considered being able to predict $\text{SFe(III)}_{\text{app}}$ to within 58 % of the determined DFe concentration as encouraging and hence further examined the temporal and spatial variability of Fe species calculated at ambient pH, DFe and DOC in the Celtic Sea.

770 4.3.3 Calculated Fe speciation at ambient pH and temperature in the Celtic Sea

We examined spatial and temporal variability in Fe speciation that results from changes in DFe and pH in our study region using parameter set D. However, we note that the differences in both calculated $\text{pFe(III)}'$ and $\text{SFe(III)}_{\text{app}}$ between A and D were limited (maximum for $\text{pFe(III)}'$ of 1.2
775 log units and 0.2 nmol L^{-1} for $\text{SFe(III)}_{\text{app}}$), especially at low DOC concentrations (negligible for $\text{pFe(III)}'$ and 0.05 nmol L^{-1} for $\text{SFe(III)}_{\text{app}}$). We re-calculated Fe speciation using ambient DFe concentrations and allowed for formation of $\text{Fe(OH)}_3(\text{s})$ where $\text{DFe} > \text{SFe(III)}_{\text{app}}$. We first examined the temporal variability in $\text{SFe(III)}_{\text{app}}$ and $\text{pFe(III)}'$ on the Celtic Sea Shelf and then spatiotemporal variation across the shelf break using i) ambient DOC and ii) a fixed DOC
780 concentration set to the lowest deep-water DOC concentration observed in our study area ($43.7 \mu\text{mol L}^{-1}$).

4.3.3.1 Seasonal variability in the Central Celtic Sea (site CCS) on the shelf.

785 The hydrography and the seasonal cycles of DFe, DOC and pH of the Celtic Sea during our sampling period has been described in detail elsewhere (Birchill et al., 2017; Carr et al., 2018; Humphreys et al., 2019; Rusiecka et al., 2018). Briefly, DFe concentrations varied both in the surface mixed layer and deeper waters, with the spring bloom resulting in significant drawdown of DFe in surface waters ($0.08 \pm 0.01 \text{ nmol L}^{-1}$, $n = 2$) to levels similar to observations in open
790 ocean regions, while in deeper waters DFe increased from 0.82 ± 0.02 , $n = 3$ (April) to $1.48 \pm 0.06 \text{ nmol L}^{-1}$, $n = 3$ (July) (Birchill et al., 2017). In the surface mixed layer, DOC concentrations were highest in April ($73.3 \pm 2.9 \mu\text{mol L}^{-1}$, $n = 3$) and lowest in July ($57.7 \pm 4.0 \mu\text{mol L}^{-1}$, $n = 5$)

(Figure S4). DOC concentrations tended to decrease with increasing depth in April and November, and concentrations in all three samples below the thermocline were $64.8 \pm 0.0 \mu\text{mol L}^{-1}$ (n= 3) in April and $58.7 \pm 1.75 \mu\text{mol L}^{-1}$ (n= 4) in November. In July, the trend of DOC was opposite, such that above the thermocline DOC decreased with increasing depth, whilst higher DOC was observed below the thermocline ($67.6 \pm 4.6 \mu\text{mol L}^{-1}$, n= 2). pH was higher in surface waters compared to deeper waters during all three sampling campaigns (Figure S4). A vertical gradient in pH was observed in November with a difference of 0.11 between the surface mixed layer and below the mixed layer.

The changes in DFe, pH and temperature throughout the seasonal cycle resulted in changes in both $\text{SFe(III)}_{\text{app}}$ and $\text{pFe(III)}'$ (Figure 6). In surface waters, DFe was consistently lower than calculated $\text{SFe(III)}_{\text{app}}$ and as expected, DFe was thus undersaturated with respect to $\text{Fe(OH)}_3(\text{s})$ formation in our calculations (Figure 6a). Below the mixed layer (>75 m), remineralization of sinking organic matter in the bottom mixed layer resulted in increased DFe (Birchill et al., 2017) and formation of $\text{Fe(OH)}_3(\text{s})$ in our calculations (Figure 6a). With the constant DOC scenario, $\text{SFe(III)}_{\text{app}}$ changed by $< 0.03 \text{ nmol L}^{-1}$ at station CCS. For the ambient DOC scenario $\text{SFe(III)}_{\text{app}}$ was overall higher by 0.3 nmol L^{-1} as a result of the increased DOC concentrations (Figure S4), however variability was also low ($< 0.02 \text{ nmol L}^{-1}$). Remarkably, we found that the $\text{SFe(III)}_{\text{app}}$ determined by our speciation model for the bottom mixed layer were very similar ($0.54\text{-}0.87 \text{ nmol L}^{-1}$, Figure 6a) to the concentrations of DFe determined throughout the well-mixed water column in April ($0.82 \pm 0.04 \text{ nmol L}^{-1}$, n=6). Our results therefore suggest that when the water column is stratified, water below the mixed layer is oversaturated with Fe as a result of constant supply of DFe by remineralization. Winter mixing subsequently resets the DFe inventory to one that our results suggest could be based on Fe solubility.

Above the mixed layer, $\text{pFe(III)}'$ was primarily dependent on DFe concentrations, with pH having a minor influence (Figure 6b) because of the low degree of heterogeneity predicted by parameter set D (Figure 5b). Below the surface (>75 m), the over-saturation of Fe in July and November meant that $\text{pFe(III)}'$ was rather constant (10.04 ± 0.02) and controlled by the formation of $\text{Fe(OH)}_3(\text{s})$ in our calculations rather than by the strength of binding to organic matter. In April, surface water (<75 m) $\text{pFe(III)}'$ was similar to those in deeper waters as the water column was well-mixed, whilst a marked increase of $\text{pFe(III)}'$ was observed from surface to deeper

waters in July and November (Figure 6b). pFe(III)' was thus predicted to increase in surface
825 waters from summer through to spring in both constant and ambient DOC scenarios. The
increase in pFe(III)' was thus largely driven by the drawdown of DFe in April resulting from
phytoplankton productivity (Birchill et al., 2017). After July, the slight increase in vertical
exchange due to mixing and the on shelf circulation pattern resulted in a decrease surface water
pFe(III)' from July to November, even though the water column remained stratified.

830

4.3.3.2 Spatiotemporal variation in key variables and Fe speciation over the Shelf break

Temperature and salinity data over the shelf break are provided in Figure S5. Dissolved Fe
ranged in concentration between 0.03-1.90 nmol L⁻¹ along the transect and was lower in surface
835 waters (0.22±0.12 nmol L⁻¹ in November, 0.20±0.28 nmol L⁻¹ in July), and enhanced in deeper
waters below ~500 m (1.04±0.24 nmol L⁻¹ in November, 0.87±0.14 nmol L⁻¹ in July, Figure 7).
The distribution and concentration of DFe are broadly consistent with previous observations in
the Celtic Sea (Nedelec et al., 2007) and neighbouring Bay of Biscay (Laès et al., 2007; Ussher
et al., 2007). A notable exception is that the DFe observed in this study during July 2015 in the
840 surface mixed layer include the lowest reported DFe concentrations (< 0.1 nmol L⁻¹) for waters
in this region. These are attributed to biological Fe uptake during the spring bloom coupled with
low external inputs to the surface mixed layer (Birchill et al., 2017). In contrast to surface waters,
concentrations of DFe in excess of 1.00 nmol L⁻¹ (to a maximum of 1.90 nmol L⁻¹) were
observed at inner shelf stations in November (C03-C06, CS2) and July (C04-06) at depths >500
845 m, which we attribute to a lateral flux of DFe from the Celtic Sea shelf slope (Nedelec et al.,
2007).

Average DOC concentrations of 60.1 ± 9.2 µmol L⁻¹ (n= 48) were observed in November, and
58.4 ± 14.2 µmol L⁻¹ (n= 28) in July (Figure 7). Higher DOC concentrations were occasionally
850 observed in surface waters (station C06 in November (98.23 µmol L⁻¹) and station C02 in July
(111 µmol L⁻¹)). Between 200-1000 m, DOC was higher at C03 station than at other stations in
November, a feature that partly coincided with higher DFe concentrations. In the deep ocean (>
1000 m), DOC was slightly lower in July (49.2±3.19 µmol L⁻¹) than in November (52.3±3.3
µmol L⁻¹).

855

Surface waters in the area exhibited higher, relatively uniform pH (Figure 7). Higher surface water pH at C04-06 stations coincided with higher DOC in autumn, which suggest that both of these features were driven by increased productivity as observed at CCS. At depth (> 1000 m), changes in pH corresponded to changes in salinity and temperature and were thus likely
860 influenced by water mass circulation and the biological carbon pump (Figure S5).

For both the ambient and constant DOC scenarios, $SFe(III)_{app}$ was $>0.8 \text{ nmol L}^{-1}$ in the deep ocean (>1500 m) at stations C01 and C02 in November and July (Figure 8). Mean $SFe(III)_{app}$ (0.96 ± 0.08 and $0.88 \pm 0.08 \text{ nmol L}^{-1}$ for the ambient and constant DOC scenarios respectively)
865 was again remarkably close to the mean observed DFe concentrations ($0.9 \pm 0.1 \text{ nmol L}^{-1}$). We emphasize here that the DFe concentration is not a parameter included in the calculations of $SFe(III)_{app}$, since the total Fe concentration is set to 10 nmol L^{-1} for all samples and our calculated $SFe(III)_{app}$ concentrations are thus independent of DFe. The slight increase in predicted $SFe(III)_{app}$ as the water depth decreases over the shelf is due to the impact of both
870 decreased pH and temperature on the formation of $Fe(OH)_3(s)$ in the calculations. The potential impact of scaling to DOC concentration is illustrated by increases in the difference between $SFe(III)_{app}$ calculated where ambient DOC concentrations were high ($>70 \text{ } \mu\text{mol L}^{-1}$) relative to the assumed constant concentration scenario of $43.7 \text{ } \mu\text{mol L}^{-1}$ at stations C03-CS2 in November or at station C06 in July (Figure 8). Nevertheless the difference between $SFe(III)_{app}$ calculated at
875 constant DOC and ambient DOC was always less than 0.54 nmol^{-1} (Figure 8) and scaling to DOC thus has a limited overall impact on determined $SFe(III)_{app}$.

In surface waters, DFe was consistently lower ($<0.25 \text{ nmol L}^{-1}$) than $SFe(III)_{app}$ predicted using both DOC scenarios and Fe^{3+} was thus undersaturated with respect to $Fe(OH)_3(s)$ formation in our calculations (Figure 8), as observed for surface waters at CCS. The depth at which DFe
880 became less than $SFe(III)_{app}$ shoaled with the DFe concentration (Figure 7 and 8). In waters close to the seafloor on the inner shelf (C03-C06), DFe concentrations were in excess of the $SFe(III)_{app}$ concentration. As described for station CCS, we suggest that these waters were influenced by non-equilibrium processes. Our speciation calculations are considered to be at equilibrium and thus do not account for any non-equilibrium processes that may be occurring in the water
885 column, such as scavenging, inputs from sediments or changes in redox state. Our study region is

known to experience inputs of DFe along with other metals in nepheloid layers that propagate offshore from the sediments over the shelf break (Laès et al., 2007; Rusiecka et al., 2018), and previous work found that the authigenic or scavenged fraction of particulate Fe becomes increasingly important close to the seafloor (Marsay et al., 2017). Such sediment-derived benthic
890 inputs can be expected to be scavenged from the water column and adsorptive processes are likely to depend on particle concentrations (Bergquist and Boyle, 2006; Fitzsimmons et al., 2013; John et al., 2018). However, the mechanisms and processes governing scavenging in the ocean are poorly constrained (Boyd and Ellwood, 2010; Tagliabue et al., 2014) and scavenging rates are effectively treated as “free” parameters in biogeochemical models and thus tuned to achieve
895 realistic Fe concentrations (Tagliabue et al., 2014). Our work confirms previous studies (Hiemstra and van Riemsdijk, 2006) suggesting that the solubility of Fe is an important constraint on the extent of Fe scavenging in the ocean and that changes in pH and temperature in the deep ocean are important for setting solubility.

900 Calculated $p\text{Fe(III)'}$ was lowest in deep waters and highest in surface waters (Figure 8b, $p\text{Fe}'$ scale is reversed). Below ~500m, $p\text{Fe(III)'}$ (10.04 ± 0.02) was relatively constant throughout the water column in November and July and irrespective of the DOC scenario, largely because it is set by the solubility product of $\text{Fe(OH)}_3(\text{s})$ in our calculations (i.e. $p\text{Fe(III)'} \propto [\text{Fe}^{3+}]$ which in turn is limited by $\text{Fe(OH)}_3(\text{s})$). In surface waters, when $p\text{Fe(III)'}$ is dependant on the DFe
905 concentration, $p\text{Fe(III)'}$ increased towards the open ocean from a minimum of 10.8 (constant DOC) or 11 (ambient DOC) at C06 to a maximum of 13.2 (constant DOC) or 14.6 (ambient DOC) at C01 (Figure 8). For the stations furthest offshore, the potential impact of scaling to DOC for calculation of $p\text{Fe(III)'}$ was more important. For example, a $30 \mu\text{mol L}^{-1}$ increase in DOC resulted in an increase of two units in $p\text{Fe(III)'}$ in surface waters at station C01. We found
910 that values of $p\text{Fe(III)'}$ predicted using parameter set D under both constant and variable DOC scenarios encompassed the range of values found to support both iron-replete and iron-limited growth in families of phytoplankton including cyanophytes, haptophytes and diatoms which have been observed in our study area (Blain et al., 2004). For example, reduction in growth of *Synechococcus* sp. was shown to begin at $p\text{Fe}'$ values of 14 (Timmermans et al., 2005), close to
915 the lowest values predicted by parameter set D with ambient DOC concentrations, while Sunda & Huntsman (1995) found onset of growth was limited at 20 pmol L^{-1} ($p\text{Fe(III)'} = 10.7$) for the

small haptophyte *Emiliania huxleyi* and at 160 pmol L⁻¹ (pFe(III)' = 9.8) for the diatom *Thalassiosira weissflogii*. However, we have not considered the role of redox chemistry in our calculations. Fe(II) is known to be more readily available to phytoplankton (Shaked and Lis, 2012) and significant concentrations of Fe(II) can be formed via photochemical reduction in surface waters, with Fe(II) concentrations of up to 175 pmol L⁻¹ previously reported for surface waters (<50 m) in this region (Ussher et al., 2007).

5. Conclusions

In this work, we combined analysis of Fe speciation by AdCSV with an ion-pairing/NICA-Donnan model to determine Fe(III) speciation at equilibrium in the Celtic Sea. We first calibrated HNN in the absence of organic matter for the experimental conditions applied in our study. We then compared titration data obtained by varying both Fe concentrations and HNN concentrations with calculations of Fe speciation predicted via the NICA-Donnan model with four sets of parameters and found that the parameter sets that predicted relatively weak binding with low heterogeneity best described our titration data. We further found that fits improved on application of a constant low DOC concentration of 43.7 μmol L⁻¹ across the data set, rather than assuming that binding scaled to ambient DOC concentrations. This suggests that binding sites could be diluted by fresh inputs of DOM that result from phytoplankton productivity, and may be more strongly linked to the refractory component of marine DOM.

We used the NICA-Donnan parameters that fitted most closely to our titration data to predict SFe(III)_{app} and pFe(III)' at ambient seawater pH and temperature with both ambient and fixed DOC concentrations. Calculated SFe(III)_{app} concentrations (ca. 0.9 nmol L⁻¹) were within the range of the water column DFe concentrations observed on the shelf after winter mixing and also the furthest off-shore deep water DFe concentrations. In surface waters DFe concentrations were lower than SFe(III)_{app} as result of the drawdown of DFe by phytoplankton. On the shelf in July and November and over the shelf break DFe exceeded SFe(III)_{app} in deeper waters close to the seafloor, which could potentially be ascribed to inputs of DFe from remineralization and sediments. Although the proximity of our calculated SFe(III)_{app} to the observed DFe concentrations is very encouraging, we highlight that our calculations are a simplification of the real system since we do not account for non-equilibrium processes, and the physical size of our

SFe(III)_{app} fraction may not map directly onto the DFe concentration. Comparing the fixed and ambient DOC scenarios suggests that scaling binding site concentrations to DOC concentrations has a limited overall impact on Fe speciation and the impact was mostly restricted to situations waters where DFe concentrations are lower than SFe(III)_{app}. Since SFe(III)_{app} is controlled by the solubility of Fe(OH)₃(s), relative changes in SFe(III)_{app} will depend on both pH and temperature. In our study region, changes in temperature resulted in a potential 0.5 nmol L⁻¹ change in SFe(III)_{app}, whilst the pH range observed in our study area was too limited to detect a strong pH effect.

We also calculated pFe(III)' in our study region and predicted values between 10 and 14, a range which encompasses the range of pFe(III)' shown to limit growth in phytoplankton. The lower limit on pFe(III)' was set by the solubility of Fe(OH)₃(s). The upper limit and changes in pFe(III)' were strongly influenced by the DFe concentration, although DOC concentrations also had an impact if binding site concentrations are scaled to DOC. The limited pH range meant that pH did not have a strong influence on pFe(III)' in this study region.

We suggest that the use of intrinsic binding parameters for Fe binding to DOM has the potential to improve understanding of the influence of organic matter on Fe solubility at ambient pH and temperatures and allow for more confident disentangling of the different processes affecting the DFe inventory, although further work is required to refine NICA constants for Fe in seawater. Furthermore, our results suggest it may be possible to further simplify calculations of Fe speciation in marine waters by assuming a constant binding site concentration, at least in waters remote from terrestrial influences, although this finding should be confirmed in further work employing more sensitive analytical approaches for determination of Fe speciation than we applied in this study. A robust parameterization of the relationship between pH, DOC, temperature and DFe with respect to both Fe bioavailability and solubility also has the potential to provide for a more mechanistic description of Fe binding in global biogeochemical models.

Acknowledgement

The authors would like to thank Bert-Jan Groenenberg for his help with PEST-ORCHESTRA. We thank the captain and crew of the RSS Discovery. KZ was supported by a scholarship from the China Scholarship Council. The project was funded by the UK Natural Environment

Research Council (NE/L501840/1 (A.B.), NE/K001779/1 (M.L., S.U., A.M.), NE/K002007/1
980 (N.C and C.M.), NE/K001973/1 (E.A. and M.G.) and the Helmholtz Association. The authors
declare no competing financial interest. All data that supports the findings of this study have
been submitted to the British Oceanography Data Centre. Raw titration data can be downloaded
from dx.doi.org/10.17504/protocols.io.brc4m2yw.

985

References

- Abualhaija, M.M., van den Berg, C.M.G., 2014. Chemical speciation of iron in seawater using
catalytic cathodic stripping voltammetry with ligand competition against salicylaldehyde.
990 *Mar. Chem.* 164, 60–74. <https://doi.org/10.1016/j.marchem.2014.06.005>
- Achterberg, E.P., Steigenberger, S., Marsay, C.M., Lemoigne, F.A.C., Painter, S.C., Baker, A.R.,
Connelly, D.P., Moore, C.M., Tagliabue, A., Tanhua, T., 2018. Iron Biogeochemistry in the
High Latitude North Atlantic Ocean. *Sci. Rep.* 8, 1–15. <https://doi.org/10.1038/s41598-018-19472-1>
- 995 Ardiningsih, I., Zhu, K., Lodeiro, P., Gledhill, M., Reichart, G.-J., Achterberg, E.P., Middag, R.,
Gerringa, L.J.A., 2021. Iron Speciation in Fram Strait and Over the Northeast Greenland
Shelf: An Inter-Comparison Study of Voltammetric Methods. *Front. Mar. Sci.* 7, 1203.
<https://doi.org/10.3389/fmars.2020.609379>
- Avendaño, L., Gledhill, M., Achterberg, E.P., Rérolle, V.M.C., Schlosser, C., 2016. Influence of
1000 ocean acidification on the organic complexation of iron and copper in Northwest European
shelf seas; a combined observational and model study. *Front. Mar. Sci.* 3, 58.
<https://doi.org/10.3389/fmars.2016.00058>
- Barbeau, K., Photochemistry, S., Barbeau, K., 2006. Photochemistry of Organic Iron (III)
Complexing Ligands in Oceanic Systems Invited Review Photochemistry of Organic Iron
1005 (III) Complexing Ligands in Oceanic Systems. *Photochem. Photobiol.* 82, 1505–1516.
<https://doi.org/10.1562/2006-06-16-IR-935>
- Barrón, C., Duarte, C.M., 2015. Dissolved organic carbon pools and export from the coastal
ocean. *Global Biogeochem. Cycles* 29, 1725–1738. <https://doi.org/10.1002/2014GB005056>
- Benedetti, M.F., van Riemsdijk, W.H., Koopal, L.K., 1996. Humic Substances Considered as a

- 1010 Heterogeneous Donnan Gel Phase. <https://doi.org/10.1021/ES950012Y>
- Bergquist, B.A., Boyle, E.A., 2006. Dissolved iron in the tropical and subtropical Atlantic Ocean. *Global Biogeochem. Cycles* 20. <https://doi.org/10.1029/2005GB002505>
- Birchill, A.J., Milne, A., Woodward, E.M.S., Harris, C., Annett, A., Rusiecka, D., Achterberg, E.P., Gledhill, M., Ussher, S.J., Worsfold, P.J., Geibert, W., Lohan, M.C., 2017. Seasonal iron depletion in temperate shelf seas. *Geophys. Res. Lett.* 44, 8987–8996. <https://doi.org/10.1002/2017GL073881>
- 1015 Blain, S., Guieu, C., Claustre, H., Leblanc, K., Moutin, T., Quéguiner, B., Ras, J., Sarthou, G., 2004. Availability of iron and major nutrients for phytoplankton in the northeast Atlantic Ocean. *Limnol. Oceanogr.* 49, 2095–2104. <https://doi.org/10.4319/lo.2004.49.6.2095>
- 1020 Boyd, P.W., Ellwood, M.J., 2010. The biogeochemical cycle of iron in the ocean. *Nat. Geosci.* 3, 675–682. <https://doi.org/10.1038/ngeo964>
- Boyd, P.W., Jickells, T., Law, C.S., Blain, S., Boyle, E.A., Buesseler, K.O., Coale, K.H., Cullen, J.J., de Baar, H.J.W., Follows, M., Harvey, M., Lancelot, C., Levasseur, M., Owens, N.P.J., Pollard, R., Rivkin, R.B., Sarmiento, J., Schoemann, V., Smetacek, V., Takeda, S., Tsuda, A., Turner, S., Watson, A.J., 2007. Mesoscale iron enrichment experiments 1993-2005: Synthesis and future directions. *Science* (80-). 315, 612–617.
- 1025 Boye, M., Aldrich, A.P., van den Berg, C.M.G., de Jong, J.T.M., Veldhuis, M., de Baar, H.J.W., 2003. Horizontal gradient of the chemical speciation of iron in surface waters of the northeast Atlantic Ocean. *Mar. Chem.* 80, 129–143.
- 1030 Boye, M., van den Berg, C.M.G., de Jong, J.T.M., Leach, H., Croot, P., de Baar, H.J.W., 2001. Organic complexation of iron in the Southern Ocean. *Deep. Res. Part I-Oceanographic Res. Pap.* 48, 1477–1497.
- Buck, K.N., Moffett, J., Barbeau, K.A., Bundy, R.M., Kondo, Y., Wu, J., 2012. The organic complexation of iron and copper: an intercomparison of competitive ligand exchange-adsorptive cathodic stripping voltammetry (CLE-ACSV) techniques. *Limnol. Oceanogr. Methods* 10, 496–515. <https://doi.org/10.4319/lom.2012.10.496>
- 1035 Buck, K.N., Sedwick, P.N., Sohst, B., Carlson, C.A., 2018. Organic complexation of iron in the eastern tropical South Pacific: Results from US GEOTRACES Eastern Pacific Zonal Transect (GEOTRACES cruise GP16). *Mar. Chem.* 201, 229–241. <https://doi.org/10.1016/J.MARCHEM.2017.11.007>
- 1040

- Buck, K.N., Sohst, B., Sedwick, P.N., 2015. The organic complexation of dissolved iron along the U.S. GEOTRACES (GA03) North Atlantic Section. *Deep. Res. Part II Top. Stud. Oceanogr.* 116, 152–165. <https://doi.org/10.1016/j.dsr2.2014.11.016>
- 1045 Byrne, R.H., Kester, D.R., 1976. Solubility of hydrous ferric oxide and iron speciation in seawater. *Mar. Chem.* 4, 255–274.
- Byrne, R.H., Luo, Y.-R.R., Young, R.W., 2000. Iron hydrolysis and solubility revisited: observations and comments on iron hydrolysis characterizations. *Mar. Chem.* 70, 23–35. [https://doi.org/10.1016/S0304-4203\(00\)00012-8](https://doi.org/10.1016/S0304-4203(00)00012-8)
- 1050 Caprara, S., Buck, K.N., Gerringa, L., Rijkenberg, M., Monticelli, D., 2016. A compilation of iron speciation data for open oceanic waters. *Front. Mar. Sci.* 3, 221. <https://doi.org/10.3389/FMARS.2016.00221>
- Carr, N., Davis, C.E., Blackbird, S., Daniels, L.R., Preece, C., Woodward, M., Mahaffey, C., 2018. Seasonal and spatial variability in the optical characteristics of DOM in a temperate shelf sea. *Prog. Oceanogr.* <https://doi.org/10.1016/J.POCEAN.2018.02.025>
- 1055 Cismasu, A.C., Michel, F.M., Tcaciuc, A.P., Tyliczszak, T., Brown Jr, G.E., 2011. Composition and structural aspects of naturally occurring ferrihydrite. *Comptes Rendus Geosci.* 343, 210–218.
- Cutter, G., Casciotti, K., Croot, P., Geibert, W., Heimbürger, L.-E., Lohan, M., Planquette, H., van de Flierdt, T., 2017. Sampling and Sample-handling Protocols for GEOTRACES Cruises. Version 3, August 2017. 139pp. & Appendices. <https://doi.org/http://dx.doi.org/10.25607/OBP-2>
- 1060 Davis, C.E., Blackbird, S., Wolff, G., Woodward, M., Mahaffey, C., 2018. Seasonal organic matter dynamics in a temperate shelf sea. *Prog. Oceanogr.* <https://doi.org/10.1016/J.POCEAN.2018.02.021>
- 1065 Dickson, A.G., 2010. Part 1 : Seawater carbonate chemistry The carbon dioxide system in seawater : equilibrium chemistry and measurements. *Guid. to best Pract. Ocean Acidif. Res. data Report.* 1–40. <https://doi.org/10.2777/66906>
- Dickson, A.G., 1990. Standard potential of the reaction: $\text{AgCl(s)} + 12\text{H}_2\text{(g)} = \text{Ag(s)} + \text{HCl(aq)}$, and the standard acidity constant of the ion HSO_4^- in synthetic sea water from 273.15 to 318.15 K. *J. Chem. Thermodyn.* 22, 113–127. [https://doi.org/http://dx.doi.org/10.1016/0021-9614\(90\)90074-Z](https://doi.org/http://dx.doi.org/10.1016/0021-9614(90)90074-Z)
- 1070

- Dickson, A.G., Millero, F.J., 1987. A comparison of the equilibrium constants for the dissociation of carbonic acid in seawater media. *Deep Sea Res.* 34, 1733–1743.
- Doherty, J., 2019. PEST, Model-Independent Parameter Estimation, User Manual Part I.
- 1075 Fitzsimmons, J.N., John, S.G., Marsay, C.M., Hoffman, C.L., Nicholas, S.L., Toner, B.M., German, C.R., Sherrell, R.M., 2017. Iron persistence in a distal hydrothermal plume supported by dissolved-particulate exchange. *Nat. Geosci.* 10, 195–201.
<https://doi.org/10.1038/ngeo2900>
- Fitzsimmons, J.N., Zhang, R., Boyle, E.A., 2013. Dissolved iron in the tropical North Atlantic
1080 Ocean. *Mar. Chem.* 154, 87–99. <https://doi.org/10.1016/j.marchem.2013.05.009>
- Gerringa, L.J.A., Rijkenberg, M.J.A., Schoemann, V., Laan, P., de Baar, H.J.W., 2015. Organic complexation of iron in the West Atlantic Ocean. *Mar. Chem.* 177, 434–446.
<https://doi.org/10.1016/j.marchem.2015.04.007>
- Gledhill, M., Achterberg, E.P., Li, K., Mohamed, K.N., Rijkenberg, M.J.A., 2015. Influence of
1085 ocean acidification on the complexation of iron and copper by organic ligands in estuarine waters. *Mar. Chem.* 177, 421–433.
<https://doi.org/http://dx.doi.org/10.1016/j.marchem.2015.03.016>
- Gledhill, M., Buck, K.N., 2012. The organic complexation of iron in the marine environment: A review. *Front. Microbiol.* 3, 69. <https://doi.org/10.3389/fmicb.2012.00069>
- 1090 Gledhill, M., Gerringa, L.J.A., 2017. The effect of metal concentration on the parameters derived from complexometric titrations of trace elements in seawater—a model study. *Front. Mar. Sci.* 4, 254. <https://doi.org/10.3389/fmars.2017.00254>
- Gledhill, M., van den Berg, C.M.G., 1994. Determination of complexation of iron(III) with natural organic complexing ligands in seawater using cathodic stripping voltammetry. *Mar. Chem.* 47, 41–54. [https://doi.org/10.1016/0304-4203\(94\)90012-4](https://doi.org/10.1016/0304-4203(94)90012-4)
- 1095 Gustafsson, J.P., 2001. Modeling the acid–base properties and metal complexation of humic substances with the Stockholm Humic Model. *J. Colloid Interface Sci.* 244, 102–112.
<https://doi.org/http://dx.doi.org/10.1006/jcis.2001.7871>
- Hansell, D.A., 2013. Recalcitrant Dissolved Organic Carbon Fractions. *Ann. Rev. Mar. Sci.* 5,
1100 421–445. <https://doi.org/10.1146/annurev-marine-120710-100757>
- Hassler, C.S., Alasonati, E., Nichols, C.A.M., Slaveykova, V.I., 2011a. Exopolysaccharides produced by bacteria isolated from the pelagic Southern Ocean - Role in Fe binding,

- chemical reactivity, and bioavailability. *Mar. Chem.* 123, 88–98.
<https://doi.org/10.1016/j.marchem.2010.10.003>
- 1105 Hassler, C.S., Schoemann, V., Nichols, C.M., Butler, E.C. V, Boyd, P.W., 2011b. Saccharides enhance iron bioavailability to Southern Ocean phytoplankton. *Proc. Natl. Acad. Sci. U. S. A.* 108, 1076–1081. <https://doi.org/10.1073/pnas.1010963108>
- Hiemstra, T., van Riemsdijk, W.H., 2006. Biogeochemical speciation of Fe in ocean water. *Mar. Chem.* 102, 181–197. <https://doi.org/10.1016/j.marchem.2006.03.008>
- 1110 Hogle, S.L., Dupont, C.L., Hopkinson, B.M., King, A.L., Buck, K.N., Roe, K.L., Stuart, R.K., Allen, A.E., Mann, E.L., Johnson, Z.I., Barbeau, K.A., 2018. Pervasive iron limitation at subsurface chlorophyll maxima of the California Current. *Proc. Natl. Acad. Sci. U. S. A.* 115, 13300–13305. <https://doi.org/10.1073/pnas.1813192115>
- Hudson, R.J.M., Rue, E.L., Bruland, K.W., 2003. Modeling complexometric titrations of natural
1115 water samples. *Environ. Sci. Technol.* 37, 1553–1562. <https://doi.org/10.1021/es025751a>
- Humphreys, M.P., Achterberg, E.P., Hopkins, J.E., Chowdhury, M.Z.H., Griffiths, A.M., Hartman, S.E., Hull, T., Smilenova, A., Wihsgott, J.U., Woodward, E.M.S., Moore, C.M., 2019. Mechanisms for a nutrient-conserving carbon pump in a seasonally stratified, temperate continental shelf sea. *Prog. Oceanogr.* 177.
1120 <https://doi.org/10.1016/j.pocean.2018.05.001>
- Hunter, K.A., Boyd, P.W., 2007. Iron-binding ligands and their role in the ocean biogeochemistry of iron. *Environ. Chem.* 4, 221–232. <https://doi.org/10.1071/en07012> | issn 1448-2517
- Hutchins, D.A., Boyd, P.W., 2016. Marine phytoplankton and the changing ocean iron cycle.
1125 *Nat. Clim. Chang.* 6, 1072–1079. <https://doi.org/10.1038/nclimate3147>
- Hutchins, D.A., Bruland, K.W., 1998. Iron-limited diatom growth and Si:N uptake ratios in a coastal upwelling regime. *Nature* 393, 561–564. <https://doi.org/10.1038/31203>
- Hutchins, D.A., Witter, A.E., Butler, A., Luther III, G.W., 1999. Competition among marine phytoplankton for different chelated iron species. *Nature* 400, 858–861.
- 1130 Janney, D.E., Cowley, J.M., Buseck, P.R., 2000. Transmission Electron Microscopy of Synthetic 2- and 6-Line Ferrihydrite. *Clays Clay Miner.* 48, 111–119.
<https://doi.org/10.1346/CCMN.2000.0480114>
- Janot, N., Pinheiro, J.P., Botero, W.G., Meeussen, J.C.L., Groenenberg, J.E., 2017. PEST-

- ORCHESTRA, a tool for optimising advanced ion-binding model parameters: Derivation of
1135 NICA-Donnan model parameters for humic substances reactivity. *Environ. Chem.* 14, 31–
38. <https://doi.org/10.1071/EN16039>
- John, S.G., Helgoe, J., Townsend, E., Weber, T., DeVries, T., Tagliabue, A., Moore, K., Lam, P.,
Marsay, C.M., Till, C., 2018. Biogeochemical cycling of Fe and Fe stable isotopes in the
Eastern Tropical South Pacific. *Mar. Chem.* 201, 66–76.
1140 <https://doi.org/10.1016/j.marchem.2017.06.003>
- Johnson, K.S., Gordon, R.M., Coale, K.H., 1997. What controls dissolved iron in the world
ocean? *Mar. Chem.* 57, 137–161.
- Kinniburgh, D.G., van Riemsdijk, W.H., Koopal, L.K., Borkovec, M., Benedetti, M.F., Avena,
M.J., 1999. Ion binding to natural organic matter: competition, heterogeneity, stoichiometry
1145 and thermodynamic consistency. *Colloids Surfaces A Physicochem. Eng. Asp.* 151, 147–
166. [https://doi.org/http://dx.doi.org/10.1016/S0927-7757\(98\)00637-2](https://doi.org/http://dx.doi.org/10.1016/S0927-7757(98)00637-2)
- Koch, B.P., Ludwichowski, K.U., Kattner, G., Dittmar, T., Witt, M., 2008. Advanced
characterization of marine dissolved organic matter by combining reversed-phase liquid
chromatography and FT-ICR-MS. *Mar. Chem.* 111, 233–241.
1150 <https://doi.org/10.1016/j.marchem.2008.05.008>
- Kogut, M.B., Voelker, B.M., 2001. Strong copper-binding behavior of terrestrial humic
substances in seawater. *Environ. Sci. Technol.* 35, 1149–1156.
<https://doi.org/10.1021/es0014584>
- Kuma, K., Isoda, Y., Nakabayashi, S., 2003. Control on dissolved iron concentrations in deep
1155 waters in the western North Pacific: Iron (III) hydroxide solubility. *J. Geophys. Res. C*
Ocean. 108, 5–1. <https://doi.org/10.1029/2002jc001481>
- Kuma, K., Katsumoto, A., Kawakami, H., Takatori, F., Matsunaga, K., 1998. Spatial variability
of Fe(III) hydroxide solubility in the water column of the northern North Pacific Ocean.
Deep. Res. 45, 91–113.
- 1160 Kuma, K., Katsumoto, A., Shiga, N., Sawabe, T., Matsunaga, K., 2000. Variation of size-
fractionated Fe concentrations and Fe(III) hydroxide solubilities during a spring
phytoplankton bloom in Funka Bay (Japan). *Mar. Chem.* 71, 111–123.
[https://doi.org/10.1016/S0304-4203\(00\)00044-X](https://doi.org/10.1016/S0304-4203(00)00044-X)
- Kuma, K., Nishioka, J., Matsunaga, K., 1996. Controls on iron(III) hydroxide solubility in

- 1165 seawater: The influence of pH and natural organic chelators. *Limnol. Oceanogr.* 41, 396–407.
- Laës, A., Blain, S., Laan, P., Ussher, S.J.J., Achterberg, E.P.E.P., Tréguer, P., De Baar, H.J.W.J.W.W., Laës, A., Blain, S., Laan, P., Ussher, S.J.J., Achterberg, E.P.E.P., Tréguer, P., De Baar, H.J.W.J.W.W., Laes, A., Blain, S., Laan, P., Ussher, S.J.J., Achterberg, E.P.E.P., Treguer, P., De Baar, H.J.W.J.W.W., 2007. Sources and transport of dissolved iron and manganese along the continental margin of the Bay of Biscay. *Biogeosciences (BG)* 4, 181–194. <https://doi.org/10.5194/bg-4-181-2007>
- 1170 Laglera, L.M., Battaglia, G., van den Berg, C.M.G., 2011. Effect of humic substances on the iron speciation in natural waters by CLE/CSV. *Mar. Chem.* 127, 134–143. <https://doi.org/10.1016/j.marchem.2011.09.003>
- 1175 Laglera, L.M., Filella, M., 2015. The relevance of ligand exchange kinetics in the measurement of iron speciation by CLE–AdCSV in seawater. *Mar. Chem.* 173, 100–113. <https://doi.org/10.1016/j.marchem.2014.09.005>
- Laglera, L.M., van den Berg, C.M.G., 2009. Evidence for geochemical control of iron by humic substances in seawater. *Limnol. Oceanogr.* 54, 610–619.
- 1180 Liu, X., Millero, F.J., 2002. The solubility of iron in seawater. *Mar. Chem.* 77, 43–54. [https://doi.org/10.1016/S0304-4203\(01\)00074-3](https://doi.org/10.1016/S0304-4203(01)00074-3)
- Liu, X., Millero, F.J., 1999. The solubility of iron hydroxide in sodium chloride solutions. *Geochim. Cosmochim. Acta* 63, 3487–3497. [https://doi.org/http://dx.doi.org/10.1016/S0016-7037\(99\)00270-7](https://doi.org/http://dx.doi.org/10.1016/S0016-7037(99)00270-7)
- 1185 Lodeiro, P., Rey-Castro, C., David, C., Achterberg, E.P., Puy, J., Gledhill, M., 2020. Acid-base properties of dissolved organic matter extracted from the marine environment. *Sci. Total Environ.* 729, 138437. <https://doi.org/10.1016/j.scitotenv.2020.138437>
- Lønborg, C., Carreira, C., Jickells, T., Álvarez-Salgado, X.A., 2020. Impacts of Global Change on Ocean Dissolved Organic Carbon (DOC) Cycling. *Front. Mar. Sci.* 7, 466. <https://doi.org/10.3389/fmars.2020.00466>
- 1190 Marsay, C.M., Barrett, P.M., McGillicuddy, D.J., Sedwick, P.N., 2017. Distributions, sources, and transformations of dissolved and particulate iron on the Ross Sea continental shelf during summer. *J. Geophys. Res. Ocean.* 122, 6371–6393. <https://doi.org/10.1002/2017JC013068>
- 1195

- Mawji, E., Gledhill, M., Milton, J.A.J.A., Zubkov, M.V.M. V, Thompson, A., Wolff, G.A.G.A., Achterberg, E.P.E.P., 2011. Production of siderophore type chelates in Atlantic Ocean waters enriched with different carbon and nitrogen sources. *Mar. Chem.* 124, 90–99. <https://doi.org/10.1016/j.marchem.2010.12.005>
- 1200 Meeussen, J.C.L., 2003. Orchestra: An object-oriented framework for implementing chemical equilibrium models. *Environ. Sci. Technol.* 37, 1175–1182. <https://doi.org/10.1021/es025597s>
- Mehrbach, C., Culberson, C.H., Hawley, J.E., Pytkowicz, R.M., 1973. Measurement of the apparent dissociation constants of carbonic acid in seawater at atmospheric pressure. *Limnol. Oceanogr.* 18, 897–906.
- 1205 Millero, F.J., Woosley, R., Ditrolio, B., Waters, J., 2009. Effect of Ocean Acidification on the Speciation of Metals in Seawater. *Oceanography* 22, 72–85.
- Milne, C.J., Kinniburgh, D.G., Tipping, E., 2001. Generic NICA-Donnan model parameters for proton binding by humic substances. *Environ. Sci. Technol.* 35, 2049–2059. <https://doi.org/10.1021/es000123j>
- 1210 Milne, C.J., Kinniburgh, D.G., Van Riemsdijk, W.H., Tipping, E., 2003. Generic NICA - Donnan model parameters for metal-ion binding by humic substances. *Environ. Sci. Technol.* 37, 958–971. <https://doi.org/10.1021/es0258879>
- Muller-Karger, F.E., Varela, R., Thunell, R., Luerssen, R., Hu, C., Walsh, J.J., 2005. The importance of continental margins in the global carbon cycle. *Geophys. Res. Lett.* 32, 1–4. <https://doi.org/10.1029/2004GL021346>
- 1215 Muller, F.L.L., 2018. Exploring the potential role of terrestrially derived humic substances in the marine biogeochemistry of iron. *Front. Earth Sci.* 6, 1–20. <https://doi.org/10.3389/feart.2018.00159>
- 1220 Ndungu, K., 2012. Model predictions of copper speciation in coastal water compared to measurements by analytical voltammetry. *Environ. Sci. Technol.* 46, 7644–7652. <https://doi.org/10.1021/es301017x>
- Nedelec, F., Statham, P.J., Mowlem, M., 2007. Processes influencing dissolved iron distributions below the surface at the Atlantic Ocean-Celtic Sea shelf edge. *Mar. Chem.* 104, 156–170. <https://doi.org/10.1016/j.marchem.2006.10.011>
- 1225 Obata, H., Karatani, H., Nakayama, E., 1993. Automated-determination of iron in seawater by

- chelating resin concentration and chemiluminescence detection. *Anal. Chem.* 65, 1524–1528.
- 1230 Pierrot, D., Lewis, E., Wallace, D.W.R., 2006. MS Excel program developed for CO₂ system calculations. ORNL/CDIAC-105a. Carbon Dioxide Inf. Anal. Center, Oak Ridge Natl. Lab. US Dep. Energy, Oak Ridge, Tennessee.
- 1235 Pinheiro, J.P., Rotureau, E., Duval, J.F.L., 2021. Addressing the electrostatic component of protons binding to aquatic nanoparticles beyond the Non-Ideal Competitive Adsorption (NICA)-Donnan level: Theory and application to analysis of proton titration data for humic matter. *J. Colloid Interface Sci.* 583, 642–651. <https://doi.org/10.1016/j.jcis.2020.09.059>
- 1240 Pižeta, I., Sander, S.G., Hudson, R.J.M., Omanović, D., Baars, O., Barbeau, K.A., Buck, K.N., Bundy, R.M., Carrasco, G., Croot, P.L., Garnier, C., Gerringa, L.J.A., Gledhill, M., Hirose, K., Kondo, Y., Laglera, L.M., Nuester, J., Rijkenberg, M.J.A., Takeda, S., Twining, B.S., Wells, M., 2015. Interpretation of complexometric titration data: An intercomparison of methods for estimating models of trace metal complexation by natural organic ligands. *Mar. Chem.* 173, 3–24. <https://doi.org/10.1016/j.marchem.2015.03.006>
- 1245 Poorvin, L., Sander, S.G., Velasquez, I., Ibisani, E., LeClerc, G.R., Wilhelm, S.W., 2011. A comparison of Fe bioavailability and binding of a catecholate siderophore with virus-mediated lysates from the marine bacterium *Vibrio alginolyticus* PWH3a. *J. Exp. Mar. Bio. Ecol.* 399, 43–47. <https://doi.org/10.1016/j.jembe.2011.01.016>
- Ringbom, A., Still, E., 1972. The calculation and use of a coefficients. *Anal. Chim. Acta* 59, 143–146.
- 1250 Rose, A.L., Waite, T.D., 2005. Reduction of organically complexed ferric iron by superoxide in a simulated natural water. *Environ. Sci. Technol.* 39, 2645–2650. <https://doi.org/10.1021/es048765k>
- Rusiecka, D., Gledhill, M., Milne, A., Achterberg, E.P., Annett, A.L., Atkinson, S., Birchill, A., Karstensen, J., Lohan, M., Mariez, C., Middag, R., Rolison, J.M., Tanhua, T., Ussher, S., Connelly, D., 2018. Anthropogenic Signatures of Lead in the Northeast Atlantic. *Geophys. Res. Lett.* 45, 2734–2743. <https://doi.org/10.1002/2017GL076825>
- 1255 Sander, S.G., Hunter, K.A., Harms, H., Wells, M., 2011. Numerical approach to speciation and estimation of parameters used in modeling trace metal bioavailability. *Environ. Sci. Technol.* 45, 6388–6395. <https://doi.org/10.1021/es200113v>

- Schlosser, C., Streu, P., Frank, M., Lavik, G., Croot, P.L., Dengler, M., Achterberg, E.P., 2018. H₂S events in the Peruvian oxygen minimum zone facilitate enhanced dissolved Fe concentrations. *Sci. Rep.* 8, 12642. <https://doi.org/10.1038/s41598-018-30580-w>
- 1260 Shaked, Y., Lis, H., 2012. Disassembling iron availability to phytoplankton. *Front. Microbiol.* 3, 123. <https://doi.org/10.3389/fmicb.2012.00123>
- Shi, D., Xu, Y., Hopkinson, B.M., Morel, F.M.M., 2010. Effect of ocean acidification on iron availability to marine phytoplankton. *Science* (80-.). 327, 676–679.
- 1265 <https://doi.org/10.1126/science.1183517>
- Smith, R.M., Martell, A.E., Motekaitis, R.J., 2004. NIST critically selected stability constants of metal complexes database. NIST Stand. Ref. Database 46 National Institute of Standard and Technology, Ga.
- Stockdale, A., Tipping, E., Hamilton-Taylor, J., Lofts, S., 2011. Trace metals in the open oceans: Speciation modelling based on humic-type ligands. *Environ. Chem.* 8, 304–319.
- 1270 <https://doi.org/10.1071/EN11004>
- Stockdale, A., Tipping, E., Lofts, S., 2015. Dissolved trace metal speciation in estuarine and coastal waters: Comparison of WHAM/Model VII predictions with analytical results. *Environ. Toxicol. Chem.* 34, 53–63. <https://doi.org/10.1002/etc.2789>
- 1275 Stockdale, A., Tipping, E., Lofts, S., Mortimer, R.J.G., 2016. Effect of Ocean Acidification on Organic and Inorganic Speciation of Trace Metals. *Environ. Sci. Technol.* 50, 1906–1913. <https://doi.org/10.1021/acs.est.5b05624>
- Sunda, W.G., Huntsman, S.A., 1995. Iron uptake and growth limitation in oceanic and coastal phytoplankton. *Mar. Chem.* 50, 189–206. [https://doi.org/10.1016/0304-4203\(95\)00035-P](https://doi.org/10.1016/0304-4203(95)00035-P)
- 1280 Tagliabue, A., Aumont, O., Death, R., Dunne, J.P., Dutkiewicz, S., Galbraith, E., Misumi, K., Moore, J.K., Ridgwell, A., Sherman, E., Stock, C., Vichi, M., Völker, C., Yool, A., 2016. How well do global ocean biogeochemistry models simulate dissolved iron distributions? *Global Biogeochem. Cycles* 30, 149–174. <https://doi.org/10.1002/2015GB005289>
- Tagliabue, A., Williams, R.G., Rogan, N., Achterberg, E.P., Boyd, P.W., 2014. A ventilation-based framework to explain the regeneration-scavenging balance of iron in the ocean. *Geophys. Res. Lett.* 41, 7227–7236. <https://doi.org/10.1002/2014GL061066>
- 1285 Timmermans, K.R., van der Wagt, B., Veldhuis, M.J.W., Maatman, A., de Baar, H.J.W., 2005. Physiological responses of three species of marine pico-phytoplankton to ammonium,

- phosphate, iron and light limitation. *J. Sea Res.* 53, 109–120.
- 1290 Tipping, E., Lofts, S., Sonke, J.E., 2011. Humic Ion-Binding Model VII: a revised parameterisation of cation-binding by humic substances. *Environ. Chem.* 8, 225–235. <https://doi.org/http://dx.doi.org/10.1071/EN11016>
- Tipping, E., Lofts, S., Stockdale, A., 2016. Metal speciation from stream to open ocean: Modelling v. measurement. *Environ. Chem.* 13, 464–477. <https://doi.org/10.1071/EN15111>
- 1295 Town, R.M., Filella, M., 2000. Dispelling the myths: Is the existence of L1 and L2 ligands necessary to explain metal ion speciation in natural waters? *Limnol. Oceanogr.* 45, 1341–1357.
- Turner, D.R., Achterberg, E.P., Chen, C.-T.A., Clegg, S.L., Hatje, V., Maldonado, M.T., Sander, S.G., van den Berg, C.M.G., Wells, M., 2016. Toward a quality-controlled and accessible Pitzer model for seawater and related systems. *Front. Mar. Sci.* 3, 139. <https://doi.org/10.3389/fmars.2016.00139>
- 1300 Uppström, L.R., 1974. The boron/chlorinity ratio of deep-sea water from the Pacific Ocean. *Deep Sea Res. Oceanogr. Abstr.* 21, 161–162. [https://doi.org/http://dx.doi.org/10.1016/0011-7471\(74\)90074-6](https://doi.org/http://dx.doi.org/10.1016/0011-7471(74)90074-6)
- 1305 Ussher, S.J., Worsfold, P.J., Achterberg, E.P., Laës, A., Blain, S., Laan, P., De Baar, H.J.W., 2007. Distribution and redox speciation of dissolved iron on the European continental margin. *Limnol. Oceanogr.* 52, 2530–2539. <https://doi.org/10.4319/lo.2007.52.6.2530>
- van den Berg, C.M.G., 1995. Evidence for organic complexation of iron in seawater. *Mar. Chem.* 50, 139–157. [https://doi.org/10.1016/0304-4203\(95\)00032-M](https://doi.org/10.1016/0304-4203(95)00032-M)
- 1310 van den Berg, C.M.G., 1991. Potentials and potentialities of cathodic stripping voltammetry of trace elements in natural waters. *Anal. Chim. Acta* 250, 165–276.
- van den Berg, C.M.G., Nimmo, M., Daly, P., Turner, D.R., 1990. Effects of the detection window on the determination of organic copper speciation in estuarine waters. *Anal. Chim. Acta* 232, 149–159.
- 1315 Van Leeuwen, H.P., Town, R.M., 2005. Kinetic limitations in measuring stabilities of metal complexes by competitive ligand exchange-adsorptive stripping voltammetry (CLE-AdSV). *Environ. Sci. Technol.* 39, 7217–7225. <https://doi.org/10.1021/es050367+>
- Vraspir, J.M., Butler, A., 2009. Chemistry of Marine Ligands and Siderophores. *Ann. Rev. Mar. Sci.* 1, 43–63.

- 1320 Waska, H., Koschinsky, A., Dittmar, T., 2016. Fe- and Cu-Complex Formation with Artificial Ligands Investigated by Ultra-High Resolution Fourier-Transform ion Cyclotron Resonance Mass Spectrometry (FT-ICR-MS): Implications for Natural Metal-Organic Complex Studies. *Front. Mar. Sci.* 3, 119. <https://doi.org/10.3389/fmars.2016.00119>
- 1325 Worsfold, P.J., Achterberg, E.P., Birchill, A.J., Clough, R., Leito, I., Lohan, M.C., Milne, A., Ussher, S.J., 2019. Estimating uncertainties in oceanographic trace element measurements. *Front. Mar. Sci.* 6, 1–9. <https://doi.org/10.3389/fmars.2018.00515>
- Wu, J., Luther III, G.W., 1995. Complexation of iron(III) by natural organic ligands in the Northwest Atlantic Ocean by a competitive ligand equilibration method and a kinetic approach. *Mar. Chem.* 50, 159–179.
- 1330 Wu, J., Luther III, G.W., 1994. Size-fractionated iron concentrations in the water column of the western North Atlantic Ocean. *Limnol. Oceanogr.* 39, 1119–1129. <https://doi.org/10.4319/lo.1994.39.5.1119>
- Ye, Y., Völker, C., Gledhill, M., 2020. Exploring the Iron-Binding Potential of the Ocean Using a Combined pH and DOC Parameterization. *Global Biogeochem. Cycles* 34, 1–16. <https://doi.org/10.1029/2019GB006425>
- 1335 Zhang, J., Kattner, G., Koch, B.P., 2019. Interactions of trace elements and organic ligands in seawater and implications for quantifying biogeochemical dynamics: A review. *Earth-Science Rev.* 192, 631–649. <https://doi.org/10.1016/j.earscirev.2019.03.007>
- 1340

Abbreviations

Terms	Description
$k_{FeNN_3, Fe', or Fe^{3+}}^{cond}$	Conditional stability constants describing the strength of a complex FeNN ₃ relative to inorganic Fe concentration or free Fe ³⁺ concentrations
$\alpha_{FeNN_3, Fe', or Fe^{3+}}$	Side reaction coefficient for FeNN ₃ expressed relative to inorganic Fe concentration or free Fe ³⁺ concentrations

k_{FeNN_3,H^+}^{cond}	Stability constants of HNN used in an ion pairing model, that would account for competition between NN^- , H^+ , Fe^{3+} and OH^- at the ionic strengths and pH relevant to our study
Detection window	The detection window describes the range over which competition between NN^- and binding sites (L^-) can be detected. It is traditionally defined as ± 1 or 1.5 log units of $\alpha_{FeNN_3,Fe'}$ (Van Den Berg et al., 1990)
$k_{FeL,Fe'}^{cond}$	Conditional stability constants describing the strength of a complex FeL relative to inorganic Fe concentration
$\alpha_{FeL,Fe'}$	Side reaction coefficient for metal-natural ligand expressed relative to inorganic Fe concentration
$logK_{Fe(III)1\ or\ 2}$	The median value of distribution of binding affinity of Fe(III) binding to organic matter in the NICA-Donnan model
$n_{Fe(III)1\ or\ 2}$	The non-ideal constants describe the ratio of Fe(III) to binding sites
$[Fe^{3+}]_{titration}$	Free Fe concentrations determined in titrations
$[Fe^{3+}]_{cal}$	Free Fe concentrations calculated using an ion pairing model in the absence of organic matter
$[Fe^{3+}]_{NICA}$	Free Fe concentrations calculated using the NICA-Donnan model in the presence of organic matter
$DFe^*_{titration}$	The non-labile fraction of Fe determined in titrations (i.e. total Fe – $FeNN_3$)
DFe^*_{NICA}	The non-labile fraction of Fe calculated using the NICA-Donnan model in the presence of organic matter (i.e. total Fe – $FeNN_3$)